Effects of model configuration for superparametrised long-term simulations - Implementation of a cloud resolving model in EMAC (v2.50)

Harald Rybka[1,2] and Holger Tost[1]

[1]Institute for Atmospheric Physics, Johannes Gutenberg-University, Mainz, Germany
[2]German Weather Service, Offenbach am Main, Germany

Correspondence: Harald Rybka (harald.rybka@dwd.de) and Holger Tost (tosth@uni-mainz.de)

Abstract. A new module has been implemented in the ECHAM5/MESSy Atmospheric Chemistry (EMAC) Model that simulates cloud related processes on a much smaller grid. This so called superparametrisation acts as a replacement for the convection parametrisation and large-scale cloud scheme. The concept of embedding an ensemble of cloud resolving models (CRMs) inside of each grid box of a general circulation model leads to an explicit representation of cloud dynamics.

5 The new model component is evaluated against observations and the conventional usage of EMAC using a convection parametrisation. In particular, effects of applying different configurations of the superparametrisation are analyzed in a systematical way. Consequences of changing the CRMs orientation, cell size and number of cells range from regional differences in cloud amount up to global impacts on precipitation distribution and its variability. For some edge case setups the analysed climate state of superparametrised simulations even deteriorates from the mean observed energy budget.

10 In the current model configuration different climate regimes can be formed that are mainly driven by some of the parameters of the CRM. Presently, the simulated cloud cover is at the lower edge of the CMIP5 model ensemble indicating that the hydrological overturning is too efficient. However, certain "tuning" of the current model configuration could improve the currently underestimated cloud cover, which will result in a shift of the climate.

The simulation results show that especially tropical precipitation is better represented with the superparamerisation in the 15 EMAC model configuration. Furthermore, the diurnal cycle of precipitation is heavily affected by the choice of the CRM parameters. However, despite an improvement of the representation of the continental diurnal cycle in some configurations, other parameter choices result in a deterioration compared to the reference simulation using a conventional convection parameterisation.

The ability of the superparametrisation to represent latent and sensible heat flux climatology is dependent on the chosen CRM 20 setup. Further interactions of the planetary boundary layer and the free troposphere can significantly influence cloud development on the large-scale. Therefore a careful selection of the CRM setup is recommended to compensate for computational expenses.

1 Introduction

Cloud related processes are difficult to simulate on the coarse grid of a general circulation model (GCM) and have a substantial influence on the global climate (Boucher et al., 2013). Small-scale effects like deep convection need to be parametrised in global models uncovering the problem that Earth System Models (ESMs) horizontal grid spacing requires further refinement

5   to resolve cloud formation. Uncertainties in different atmospheric fields are primarily a consequence of using parametrisations (Zhang and McFarlane, 1995; Knutti et al., 2002), which rely on a physical basis but are mostly scale dependent including an arbitrary number of simplifications and assumptions. Nowadays, computational capabilities are suitable to perform global or large-domain simulations with resolution on the order of a few kilometres (Kajikawa et al., 2016; Heinze et al., 2017) or even sub-kilometer grid spacing (Miyamoto et al., 2013). Convective-permitting simulations have shown that these model are able

10   to realistically represent the Madden-Julian oscillation (MJO) (Miura et al., 2007; Miyakawa et al., 2014), the diurnal cycle of precipitation (Sato et al., 2009; Yashiro et al., 2016) or the monsoon onset (Kajikawa et al., 2015). Resolving the total effects of small-scale atmospheric features can hardly be simulated by any GCM with parameterised physics. The dilemma with these global cloud-resolving models (GCRMs) is the simulation period that is limited by the computational expense to a couple of months nowadays. On that account coarser horizontal resolutions are necessary regarding long-term simulations e.g. climate

15   projections. A pioneer high-resolution (14 km global mesh) multi-year climate simulations has been conducted by Kodama et al. (2015). In addition to that the first coordinated long-term model intercomparison of high-resolution (at least 50 km grid-size) climate simulations is underway within the High Resolution Model Intercomparison Project (HighResMIP) (Haarsma et al., 2016) of the Coupled Model Intercomparison Project 6 (CMIP6) (Eyring et al., 2016). The former examples showed that current developments and models still use resolutions that require a convection parametrisation in order to investigate climate

20   related questions. Combining the ability to reproduce small-scale cloud dynamics by a cloud-resolving model (CRM) and perform long-term simulations with a GCM resulted in the idea of a „superparametrisation" (Grabowski and Smolarkiewicz, 1999; Grabowski, 2001; Khairoutdinov and Randall, 2001).

The concept of the superparametrisation is based on embedding an ensemble of interacting CRMs inside of each column of the GCM replacing convection and large-scale cloud parametrisations. The superparametrisation acts as a conventional parametri-

25   sation but in contrast explicitly resolving small-scale cloud dynamics on the subgrid-scale of the GCM with the exception of cloud microphysics and turbulence. The CRM domain involves periodic lateral boundary conditions and forcings of large-scale tendencies computed by the GCM are applied horizontally uniform. Finally, all small-scale effects represented by the ensemble mean of all CRMs within one GCM grid-box interact with larger-scale atmosphere circulations on the coarse grid of the host model. Consequently, no direct interactions between individual CRM cells across GCM grid boundaries are possible. The

30   computational cost of performing simulations with this framework is drastically reduced in contrast to a fully global cloud-resolving model. Including a CRM for the representation of the multitude of different types of clouds is a major step toward a more realistic representation of individual clouds and their interactions that are otherwise only achievable with high resolution models over huge domains.

After the first implementation of the superparametrisation several other institutes have followed the same approach (Subra-

manian et al., 2017; Tulich, 2015; Tao et al., 2009) and other are under way (Arakawa et al., 2011). Diverse modifications exist, which incorporate other processes or schemes within the embedded small-scale model, like a two-moment microphysical scheme, a higher order turbulence closure or including aerosol coupling (Gustafson et al., 2008; Cheng and Xu, 2013; Wang et al., 2011a, b; Minghuai et al., 2015). These studies have mainly focused on improving selected process descriptions within

5   the cloud-resolving model. This study presents an additional superparametrised GCM primarily focusing on the effects of different CRM model configurations onto the mean climate state. Multiple simulations spanning 15 months have been performed to statistically evaluate the effects of changing different aspects of the superparametrisation, i.e. orientation, grid spacing and cell number of the embedded CRM. To our knowledge this is the first attempt summarizing the effects of different configurations of the superparametrisation onto the model mean climate state.

10   This paper is organized as follows. Section 2 describes the host GCM and CRM that is used as the superparametrisation. Furthermore the coupling between the two model systems and the simulation setup is given. Section 3 examines the results of the new model system and discuss the sensitivity study comparing different superparametrised model setups. Section 4 gives a summary and conclusions.

2 Model Description

2.1 EMAC model system

Historically speaking the ECHAM/MESSy atmospheric chemistry (EMAC) model (Joeckel et al., 2010) combines the Modular Earth Submodel System (MESSy) framework with the fifth generation of the ECMWF/Hamburg (ECHAM5) climate model (Roeckner et al., 2006). Developments during the last decade have fully modularised the code into the different layers of MESSy (Joeckel et al., 2005) and split representations of atmospheric processes into their own submodels. Based on

20   that, alternative process descriptions (e.g. convection parametrisations, Tost et al., 2006) and even diverse base models (e.g. Community Earth System Model (CESM, Baumgaertner et al., 2016) or the COSMO model, Kerkweg and Jöckel, 2012) can be easily selected and compared for sensitivity climate simulations. EMAC has been used for various scientific applications regarding chemistry climate interactions from the surface to the mesosphere[1]. A complete list of available submodels is given in Table 1 in Joeckel et al., 2010.

2.2 New submodule: CRM

As mentioned in the introduction a CRM has been implemented as a new submodel to serve as a superparametrisation (SP) for EMAC. The new coupled model system is therefore shortly named SP-EMAC. The CRM component of SP-EMAC is the System for Atmospheric Modeling (SAM; described in Khairoutdinov and Randall, 2003) that describes subgrid-scale development of moist physics in each GCM grid column. It solves the nonhydrostatic dynamical equations with the anelastic

30   approximation. The prognostic variables are the liquid/ice water moist static energy, total precipitating water (rain + snow +

---

[1]see http://www.messy-interface.org/ for a recently updated list of publications featuring MESSy
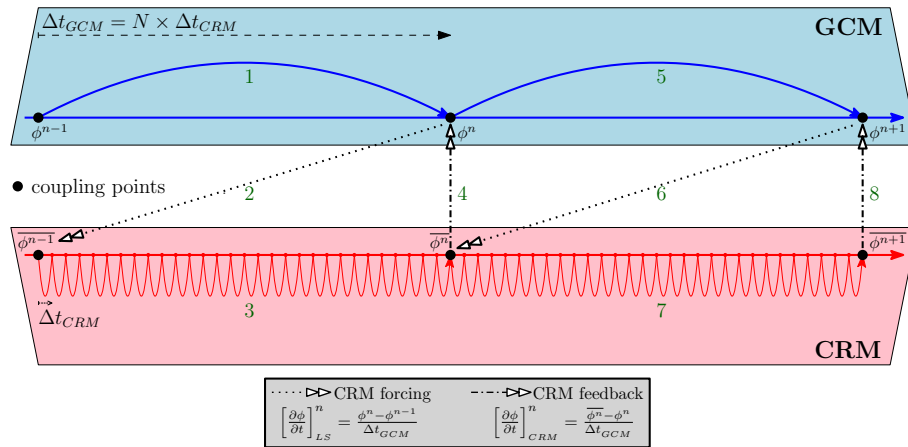
Figure 1. Sketch of model time integration when coupling a host GCM with a superparametrisation (i.e. CRM) based on their prognostic variables ϕ over a period of three time steps (n). A description of the different phases (i.e. numbers) is given in the text.

graupel) and non-precipitating water (vapor + cloud water + cloud ice). An „all-or-nothing" approach is used to diagnose cloud condensate assuming saturation with respect to water/ice. The hydrometeor partitioning is based on a temperature dependence using a single moment microphysical scheme with fixed autoconversion rates. Additional information on the CRM is described in more detail in the Appendix of Khairoutdinov and Randall (2003).

5   The model code of the superparametrisation has been re-structured to follow the MESSy coding standards. Thereby it is now possible to set specific parameters via namelist entries in order to obtain the flexibility for sensitivity analysis without recompiling the code. The main switches that can be adjusted change the configuration of the superparametrisation, i.e.:

- number of CRM grid cells inside of each GCM grid box

- grid size of CRM cells

10   - orientation of the CRM ensemble (2D or 3D)

- top height of CRM grid box

- time step of the superparametrisation

Each grid column of the global model EMAC hosts several copies of the CRM. All configurations of the superparametrisation use periodical lateral boundaries and a time step of 20 seconds. Vertical levels (29 in total) are aligned to match the lowermost

15   levels of the GCM. Newtonian damping is applied to all prognostic variables in the upper third of the grid to reduce gravity wave reflection and build up. Communication between CRM cells across GCM boundaries is done via large-scale tendencies thereby neglecting direct interactions of small-scale dynamics between coarse grid columns.

2.3 SP-EMAC: Coupling the two model systems

Combining EMAC and the superparametrisation is based on applying the CRM forcing and CRM feedback of prognostic variables ϕ between the two models. But first and foremost vertical profiles of the coarse grid cells of EMAC are initialized in all CRM columns at the beginning of each model run. Simultaneously small temperature perturbations are added for near

5 surface layers to obtain an individual response for each CRM column. During the simulation the CRM is called on every GCM time step and repeatedly integrating its equations while saving all subgrid-scale fields of the superparametrisation at the end of the call. A sketch of the GCM-CRM coupling is given in figure 1 displaying three GCM time steps (n) and their sequential phases during the model time integration. The numbers in figure 1 correspond to the following actions:

    1 $\rightarrow$ integration of GCM (time step of Δt_{GCM})

10   2 $\rightarrow$ coupling: CRM large-scale forcing $\left[\frac{\partial \phi}{\partial t}\right]_{LS}$

    3 $\rightarrow$ integration of CRM (N-times Δt_{CRM})

    4 $\rightarrow$ coupling: CRM small-scale feedback $\left[\frac{\partial \phi}{\partial t}\right]_{CRM}$

    5 to 8 $\rightarrow$ repeating phases 1 to 4

The large-scale forcing restricts the superparametrisation close to the host model fields whereas CRM feedback tendencies are

15 calculated by the ensemble horizontal mean of all CRM grid boxes ($\overline{\phi^n}$) for timestep n. Momentum transport was only allowed for the 3D CRM configurations.

With regards to the computation of cloud optical properties and radiative fluxes two possibilities exist.

1. calculate radiative transfer with averaged cloud properties assuming a maximum-random overlap assumption obtained by averaging over the superparametrisation domain.

20 2. calculate radiative transfer explicitly with time-averaged CRM fields in every subgrid-scale column.

In this paper only the first possibility is chosen although including explicit cloud inhomogeneities into radiative transfer computation have a significant influence on radiative fluxes (Cole et al., 2005). The capability to consider subgrid-scale cloud-radiation interactions have been introduced after performing sensitivity simulations and will therefore not be part of the evaluation in this paper.

25 Further coupling is not implemented in the superparametrised version of EMAC so far. All land surface fluxes are simulated on the large-scale grid only. Surface heterogeneities like soil moisture, soil type, orography etc. may be included for future research with SP-EMAC.

2.4 Simulation Setup

All simulations are performed with a horizontal GCM resolution of T42 and 31 vertical hybrid pressure levels up to 10.0 hPa.

30 The applied setup for the control simulation (CTRL) covers the submodels for radiation (Dietmüller et al., 2016), clouds

Table 1. Overview of sensitivity simulations

#	Simulation Name	Description
0	CTRL	EMAC control simulation with parametrised convection and clouds
	SP-EMAC	SP-EMAC simulations with diverse configurations specified by three abbreviations:
1	OR1 4km 64	
2	OR1 4km 32	*abbr. #1: CRM orientation*
3	OR1 4km 16	orientation of CRM cells within a GCM cell
4	OR1 2km 64	OR1, OR2 or OR3
5	OR1 2km 32	OR1 = east-west orientation
6	OR1 1km 64	OR2 = north-south orientation
7	OR1 1km 32	OR3 = three dimensional (3D) CRM
8	OR1 1km 16	
9	OR2 4km 64	*abbr. #2: CRM grid size*
10	OR2 4km 16	4km, 2km or 1km
11	OR2 2km 64	
12	OR2 2km 32	*abbr. #3: number of CRM grid cells*
13	OR2 2km 16	64, 32 or 16
14	OR2 1km 32	
15	OR3 4km 64	for the 3D orientation the CRM cells are arranged as follows:
16	OR3 4km 32	total cells = number of cells in east-west direction **x** number of cells in north-south direction
17	OR3 2km 32	64 cells = 8 **x** 8
18	OR3 2km 16	32 cells = 8 **x** 4
19	OR3 1km 64	16 cells = 4 **x** 4
20	OR3 1km 16	

(Lohmann and Roeckner, 1996) and convection (Tiedtke, 1989) with modifications of (Nordeng, 1994). Sea surface temperature (SST) and sea ice content (SIC) is prescribed by climatological monthly averaged data from the AMIP database between 1987 to 2006. This simulation is used to evaluate differences between parametrised and superparametrised climate simulations of EMAC. In order to investigate the configuration effects of the CRM several SP-EMAC runs have been performed. In each

5   SP-EMAC run an ensemble of CRMs have been embedded in each of the 8192 grid columns of the GCM. Each simulation is distinguished by its configuration of the superparametrisation. Aspects that vary along the different runs are: CRM cell orientation (OR) within a GCM grid box (alignment: north-south, east-west or full 3D), the individual size of one CRM cell (4km, 2km or 1km) and the number of CRM cells within a large-scale grid box (64, 32 or 16). Each of these three attributes characterise a SP-EMAC simulation. A list of all runs is given in table 1. Further information on the simulations setup is given

in the supplement.

The simulation period spans 15 months considering the first three months of the simulation as spin-up and discarding it from the analysis. Monthly averaged data have been used for the evaluation. In total 20 SP-EMAC simulations have been performed to evaluate the difference that come along when changing the configuration of the superparametrisation. It is noteworthy to

5 mention that no tuning is done thereby allowing the simulation to react to its own dynamics and interdependencies. This is done on purpose to derive the distinct consequence of a different CRM configuration. In order to condense the information of all superparametrised runs an ensemble depictive representation is used to display the mean performance (black line) as well as the variability (grey area) of all SP-EMAC simulations. Thereby figures always show the ensemble average of all SP-EMAC runs if not mentioned otherwise.

10 3 Evaluation

The evaluation of SP-EMAC is divided in three parts. The first section covers a global analysis of SP-EMAC comparing mean global variables and their variability. Secondly regional aspects are investigated revealing a higher importance of the CRM setup to local fields. The last part explains issues of several configurations of the superparametrisation and their impact on a global scale.

3.1 Global aspects

The first evaluation of the new model system covers the comparison of different mean global variables and their spatial and temporal distribution of SP-EMAC with the control simulation (CTRL) and several observations. Table 2 lists global mean values of top of the atmosphere (TOA) net radiative flux (F_{net}), surface temperature over land (T_s), total cloud cover (C_{tot}),

20 precipitation (P), liquid water path (LWP), ice water path (IWP) and the net cloud radiative effect (NetCRE) at TOA. These variables indicate the overall performance of all SP-EMAC simulations for the first time without tuning to relevant climate measures. Considering the radiative fluxes at TOA almost all configurations of the superparametrisation lie within a range of ± 3 W/m^2 reflecting an almost balanced radiation budget. Only three setups (OR3 4km 32, OR3 1km 64 and OR3 1km 16) show a strong negative imbalance generated by too reflective clouds. The energy deficit for these simulations can be explained

25 by a large negative net cloud radiative effect dominated in the shortwave and an overestimation of LWP. Additionally, it should be mentioned that the high imbalance are only seen for the 3D-setups of SP-EMAC. Changing the size or number of cells in a three-dimensional CRM setup drastically changes the covered area of the superparametrisation. This modification (reduction in CRM area) seems to significantly influence the CRM properties to correctly simulated the mean effects of subgrid-scale processes within a GCM cell. Another possible feedback that could degrade global statistics, affecting large-scale dynamics

30 for all OR3 simulations, is the momentum transport. Nevertheless, these simulations are discarded from further analysis because the mean climate is highly deteriorated. Concerning the range of averaged surface temperature over land (neglecting Arctic and Antarctica) values between 289 and 292 K mirror the variability of the SP-EMAC ensemble. All simulations in-

cluding the control simulations depict a higher surface temperature compared to reanalysis data. The difference is partly due to the model output variable that presents the temperature of the lowermost mode layer instead of using the 2m-temperature. More interestingly is the separation of several SP-EMAC runs into two branches divided by the criterion of an average surface temperature below 290 K (sub-ensemble A) or above 290 K (sub-ensemble B) and their annual mean precipitation of

5 above or below 3.0 mm/d. These two subsets are analysed in more detail in section 3.3. In contrast the variability in mean global precipitation occurs small. Almost all SP-EMAC configurations are within the GPCP (Global Precipitation Climatology Project) uncertainty. In a global context the CRM configuration does not have an effect on annual mean precipitation but significant differences occur spatially depending on the chosen setup (see section 3.2). The general cloud cover for all super-parameterised simulations is underestimated by 10 % with the current setup of SP-EMAC. Similar underestimations in cloud

10 amount and overestimation in cloud optical depth (see section 3.3) has been observed in past multiscale modeling framework (MMF) studies (Marchand and Ackerman, 2010). However a cloud cover around 50 % still lies within the range (at the lower end) of current estimates of several GCMs participating in the Coupled Model Intercomparison Project Phase 3 and Phase 5 (CMIP3 and CMIP5; Probst et al. (2012); Calisto et al. (2014)). Nevertheless this deficit can be compensated by further tuning efforts as it has been done for the control simulation depicting a mean cloud cover of 60 % (Mauritsen et al., 2012). Because

15 deficiencies in cloud amount are closely related to the liquid and ice water path even higher differences are expected to arise. Best estimates for globally averaged LWP (IWP) based on different observational data sets expose a highly uncertain range between 30-50 g/m^2 (25-70 g/m^2) with an upper limit of 100 g/m^2 (140 g/m^2) (Jiang et al., 2012). These differences are due to different satellite sensor sensitivities, attenuation limits, retrieval errors and algorithmic assumptions therefore showing no clear consensus throughout the literature (O'Dell et al., 2008; Stubenrauch et al., 2013). Comparing AVHHR (Advanced Very

20 High Resolution Radiometer) satellite data with model results display high discrepancies in liquid and ice partitioning. Similar to the control run all SP-EMAC configurations show a comparable mean LWP around 90 to 110 g/m^2. These high amounts of liquid water in the atmosphere are seeming to extremely overestimate the underlying observations of CM SAF (The Satellite Application Facility on Climate Monitoring) but are on the upper range of current LWP estimates and GCM simulations (Lauer and Hamilton, 2013). The physical processes during model integration of rationing cloud water into its liquid and ice phase is

25 a compensating effect on total cloud amount and radiation.

One major last aspect to consider is the net radiative effect of clouds which is affected by the total cloud cover as well as their optical thickness and vertical extent. Absorption and reflectance of solar and terrestrial radiation is influenced by the presence

Table 2. Overview of different global mean variables (values of T_s, LWP and IWP represent averages between $60°$ latitudes).

Simulation Name	F_{net} (W/m^2)	T_s (K)*	C_{tot} (%)	P (mm/d)	LWP (g/m^2)	IWP (g/m^2)	NetCRE (W/m^2)
CTRL	3.7	289.6	60.0	2.9	92	28	-22.7
OR1 4km 64	-1.7	289.1	49.7	3.1	97	53	-28.2
OR1 4km 32	-2.0	291.8	49.2	2.9	96	53	-27.2
OR1 4km 16	-3.1	291.7	51.2	2.9	102	55	-28.6
OR1 2km 64	0.6	289.5	49.9	3.1	91	56	-26.3
OR1 2km 32	0.8	291.9	50.0	2.8	90	57	-25.0
OR1 1km 64	2.2	289.4	49.5	3.1	89	57	-25.0
OR1 1km 32	-3.2	289.1	50.5	3.2	103	54	-29.8
OR1 1km 16	-1.1	289.5	53.6	3.1	100	61	-27.8
OR2 4km 64	0.3	289.5	49.6	3.1	93	53	-26.4
OR2 4km 16	-1.4	291.5	50.5	2.9	98	55	-27.1
OR2 2km 64	2.8	292.0	48.2	2.8	82	54	-23.1
OR2 2km 32	-0.1	291.8	49.0	2.9	92	54	-25.7
OR2 2km 16	0.2	291.7	50.5	2.9	94	57	-25.3
OR2 1km 32	2.8	291.8	49.5	2.8	85	57	-23.0
OR3 4km 64	-0.5	289.4	49.9	3.2	94	57	-27.4
OR3 4km 32	-7.6	291.8	54.6	2.9	110	52	-34.7
OR3 2km 32	-0.3	292.1	51.8	2.9	93	57	-27.0
OR3 2km 16	-2.0	291.7	55.1	2.9	100	60	-29.0
OR3 1km 64	-6.8	289.9	53.1	3.1	109	51	-34.5
OR3 1km 16	-11.4	289.8	59.3	3.1	124	55	-39.5
Observations	0.8 ± 0.4^a	288.9^b	62.5 ± 4.4^c	2.6 ± 0.4^d	30 ± 10^e	39 ± 20^e	-20.9 ± 4.0^a

* model average surface temperature over land is represented by values of the lowermost model layer

[a] CERES EBAF-TOA Edition 2.8 (Clouds and Earth's Radiant Energy System - Energy Balanced and Filled) - 04/2000-03/2010, Wielicki et al. (1996); Loeb et al. (2009)

[b] NCEP/DOE2 Reanalysis data provided by the NOAA/OAR/ESRL PSD, Boulder, Colorado, USA, from their Web site at https://www.esrl.noaa.gov/psd/ - 01/1979-12/2010, Kanamitsu et al. (2002)

[c] CERES ISCCP-D2LIKE-MERGED - Edition 3A, NASA Langley Atmospheric Science Data Center DAAC. DOI: 10.5067/Aqua/CERES/ISCCP-D2LIKE-MERG00_L3.003A - 04/2000-03/2010, Wong, T. (2008)

[d] Global Precipitation Climatology Project (GPCP) Climate Data Record (CDR), Version 2.3 (Monthly). National Centers for Environmental Information. DOI:10.7289/V56971M6 - 01/1981-12/2010, Adler et al. (2018)

[e] CM SAF CLARA-A2 (The Satellite Application Facility on Climate Monitoring Cloud: Albedo And Surface Radiation dataset from AVHRR data – second edition) - 04/1986-03/2010, DOI:10.5676/EUM_SAF_CM/CLARA_AVHRR/V002, Karlsson et al. (2017)

of clouds and the total net cloud radiative effect can be quantified as the sum of its shortwave and longwave component:

$$\text{NetCRE} = \text{CRE}_{\text{SW}} + \text{CRE}_{\text{LW}}$$

$$\text{CRE}_{\text{SW}} = (\text{SW}^{\downarrow} - \text{SW}^{\uparrow}_{\text{all}}) - (\text{SW}^{\downarrow} - \text{SW}^{\uparrow}_{\text{clear}})$$

$$= \text{SW}^{\uparrow}_{\text{clear}} - \text{SW}^{\uparrow}_{\text{all}}$$

5 $\quad \text{CRE}_{\text{LW}} = (\text{LW}^{\downarrow}_{\text{all}} - \text{LW}^{\uparrow}_{\text{all}}) - (\text{LW}^{\downarrow}_{\text{clear}} - \text{LW}^{\uparrow}_{\text{clear}})$

$$= \text{LW}^{\uparrow}_{\text{clear}} - \text{LW}^{\uparrow}_{\text{all}}$$

where $SW^{\uparrow}_{clear}$ and $SW^{\uparrow}_{all}$ describe the clear-sky and all-sky reflected shortwave radiation at TOA and $LW^{\uparrow}_{clear}$ and $LW^{\uparrow}_{all}$ represent clear-sky and all-sky outgoing longwave radiation (OLR) at TOA.

The NetCRE is negative describing an overall cooling effect of clouds on the atmosphere. Concerning all simulations CTRL shows with -22.7 W/m^2 a net cloud radiative effect closest to the observed value of -20.9 W/m^2. The SP-EMAC simulations

5   cover a range between -23.0 to -29.8 W/m^2 which seems even more surprising because cloud cover is highly reduced in all superparametrised simulations. This change in cloud amount would usually lead to a smaller NetCRE, which is not the case. Therefore optical properties of clouds must have substantially been changed in all SP-EMAC runs indicating an increased reflection of radiation by clouds. This is evaluated in more detail in chapter 3.3. All in all without tuning of SP-EMAC almost all CRM configurations of SP-EMAC show mean climate characteristics equivalent to the control simulation and lie within a

10 comparable range to observational estimates.

Apart from the analysis of averaged global fields figure 2 displays normalized Taylor diagrams (Taylor, 2001) for four different quantities. These type of diagrams condense various aspects of multidimensional variables in comparison to observational data in one diagram. In total the correlation (R) given by the azimuthal angle, the standard deviation (σ) which is proportional to the radial distance from the origin and the centered root-mean-square error (RMSE) corresponding to the distance from the obser-

15 vational point (which is aligned at a unit distance from the origin along the x-axis) quantify the degree of agreement between modeled and observed fields. The correlation coefficient include spatial as well as temporal correlation for all variables based upon monthly averages reflecting the pattern concurrence in time and space. In order to compare observed and simulated fields all observations are remapped onto the applied model resolution (T42 $\approx 2.8°$ at equator).

All simulations show shortwave and net radiative fluxes at TOA that are in close agreement to observed fields ($R \approx 0.98$).

20 Concerning longwave TOA radiative fluxes the correlation is slightly reduced ($R \approx 0.86$) and all SP-EMAC runs demonstrate a better variance than CTRL.

A significant improved performance in terms of correlation and variability is also visible for cloud cover reducing the centered RMSE by 10 %. The latter is a direct result of an improved representation in northern hemispheric cloud amount (not shown) whereas tropical and large ocean fractions show an underestimation in cloud cover for the superparametrised simulations. The

25 improvements in radiation and cloud amount suggest a better representation of cloud-radiation processes caused by the ability to include subgrid-scale cloud dynamics.

Comparing the continental humidity distribution for four atmospheric levels interesting features appear. Lower level specific humidity at 925 hPa show a high correlation ($R \geq 0.95$) and a comparable standard deviation for many SP-EMAC runs against reanalysis data. The underestimation of the variance ($\sigma < 0.9$) for a couple of SP-EMAC configurations comparing the lower-

30 most specific humidity fields is dependent upon temperature in the boundary layer and precipitation. All simulations with T_s above 290 K and P below 3 mm/d (compare with Table 2) display a decrease in the normalized standard deviation whereas all other SP-EMAC show a better correlation and variability. This behaviour reflects the importance of interactions between boundary layer processes and precipitating fields. An even bigger spread is visible for mid-level and upper troposphere humidity at 500 and 250 hPa. Two features are prevailing: a decrease in correlation with increasing altitude and a higher variance for

35 almost all simulations. The overestimated variability of specific humidity is mainly a cause of too much water vapor transport
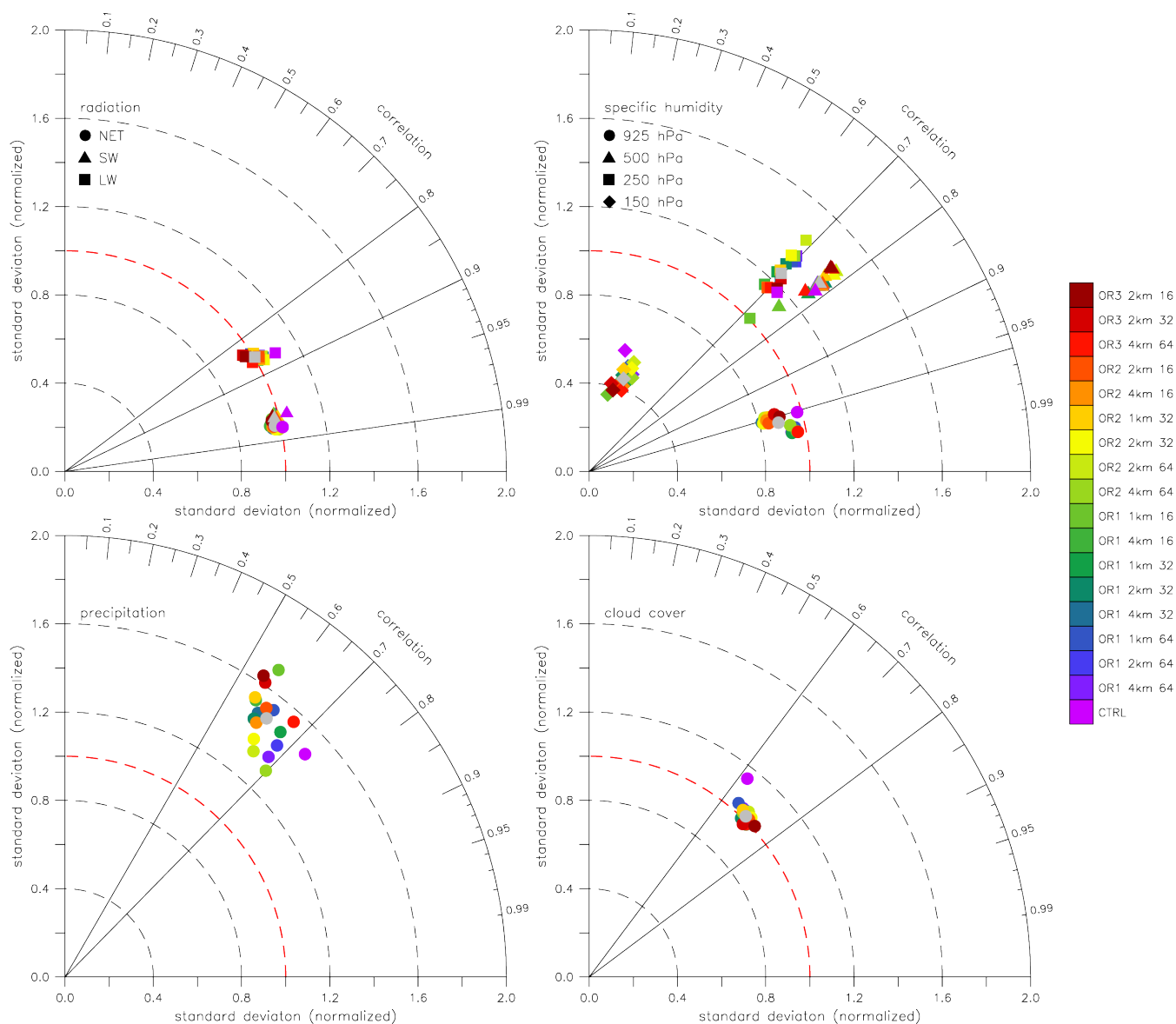
Figure 2. Taylor diagrams summarizing radiative fluxes at TOA, specific humidity on selected pressure levels, precipitation and cloud cover. Individual simulations are color-coded whereas grey markers represent the overall SP-EMAC ensemble. The control simulation is marked in purple. Observational data for radiation at TOA, cloud cover and precipitation is the same as indicated in table 2. For specific humidity NCEP/DOE2 Reanalysis data is used from 01/1979 to 12/2010 and evaluated only over continental points.

over tropical continents and too less over tropical oceans. The decrease in the correlation coefficient expresses the difficulty to simulate the appropriate water vapor transport for higher atmospheric levels especially in the intertropical convergence zone (ITCZ). Moreover, it is obvious that different SP-EMAC configurations have a strong impact on the upper tropospheric
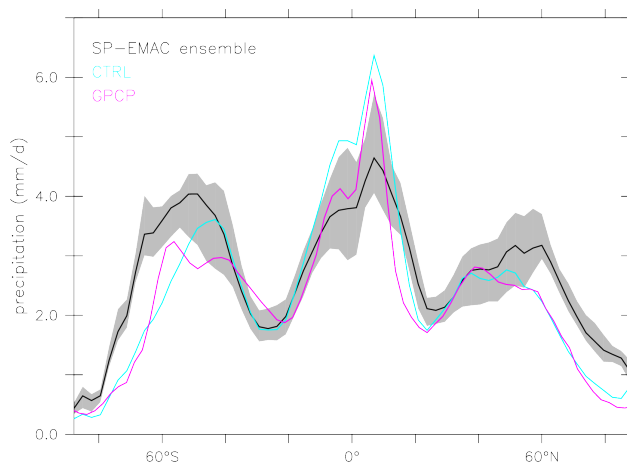
Figure 3. Zonal averaged simulated precipitation compared to GPCP data.

moisture budget at 250 hPa. This is a consequence of contrasting CRM resolved strength of vertical winds. Evaluating specific humidity distribution at the tropical tropopause level near 150 hPa almost no correlation remains and variability in these heights is strongly underestimated. This uncorrelated relationship is negatively influenced by an almost unresolved stratospheric circulation because of the sparse vertical resolution in these heights. Thereby almost no water vapour is transported from the tropics

5   to the poles.

The representation of precipitation and its spatial and temporal distribution is slightly worse compared to the CTRL simulation with correlations less than 0.7. Furthermore, the configuration of SP-EMAC strongly modifies the intensity of rainfall. A much bigger spread is visible in the Taylor diagram for precipitation comparing individual SP-EMAC runs. This pinpoints the importance of the CRM configuration onto the global precipitation distribution and will be explored in more detail focusing on

10   regional differences in the next section.

Recapitulating the evaluation of global SP-EMAC fields several Taylor diagrams show a similar spatial and temporal correlation compared to the control simulation with parametrised convection. A slightly improvement in the longwave radiative flux and cloud cover distribution is seen in the Taylor diagrams. The representation of precipitating fields is slightly deteriorated. Without the help of tuning efforts SP-EMAC could easily outperform the control simulation and thereby showing the advantage

15   of resolving small-scales features and their impact onto global metrics.

3.2   Influence on regional aspects

The introduction of a superparametrisation resolving cloud dynamics in a GCM explicitly implies changes of local phenomena like precipitation, cloud regimes or boundary layer characteristics. This section evaluates regional patterns of precipitation

20   and cloud radiative effects of SP-EMAC. In addition to that, the diurnal cycle of tropical precipitation is diagnosed as well as probability density functions (PDFs) for specified regions.
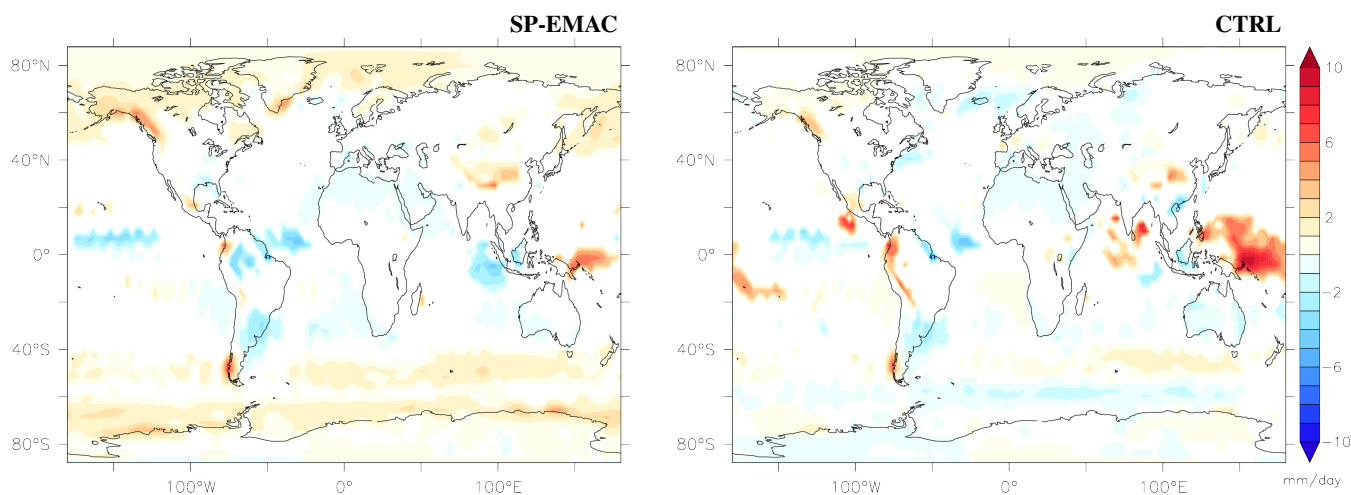
Figure 4. Differences in precipitation of SP-EMAC ensemble (left panel) and CTRL (right panel) in contrast to global observations (GPCP). Colored areas show only regions with significant differences in precipitation (analysed with t-Tests on a significance level of 90%).

As a first step, significantly different precipitating regions for all simulations are identified and compared to observations. Moreover facing current deficiencies of GCMs, two specified regions are taken into account to analyse simulated precipitation features: maritime tropics (in particular the Warm Pool region) and the southern mid-latitudes. In previous literature it has been shown that the maritime continent depicts too much precipitation for all CMIP5 models consistently (Flato et al., 2013).

5 Complementary an overestimation in oceanic precipitation frequency is simulated over the southern hemisphere indicating too much drizzle (Stephens et al., 2010). Although a new study suggested that these biases originate from processes other than convection a reduction of these errors is clearly accomplished by using convection parametrisations (Maher et al., 2018). The comparison of SP-EMAC with observations and a parametrised control simulation will reveal the importance of resolving subgrid-scale dynamics in a superparametrised GCM for these regional improvements.

10 Figure 3 shows zonal averaged precipitation rates for SP-EMAC, CTRL and GPCP data. In correspondence figure 4 highlights regions with significant differences in annual mean precipitation compared to observations. These regions have been identified by a couple of t-Tests on a significance level of 90%. For the control simulation one single t-Test has been carried out to emphasize important areas. Considering the analysis for SP-EMAC regions are highlighted when more than half of all superparametrised simulations show a significant difference between observed and modelled fields. The control simulation

15 is in close agreement to the GPCP observations with the exception of enhanced tropical precipitation, which is well represented by the superparametrisation. Contrary to this an overestimation in the northern and southern mid-latitudes is visible for SP-EMAC independent of the chosen CRM configuration. This finding is in agreement with the study of Marchand et al. (2009) showing an overestimation of low-level hydrometeors in mid-latitude storm tracks using the same superparametrisation within SP-CAM (Superparametrised - Community Atmosphere Model). An improvement is given by Kooperman et al. (2016)

20 showing no systematic biases within the mid-latitudes using a two-moment microphysical scheme linked to aerosol processes
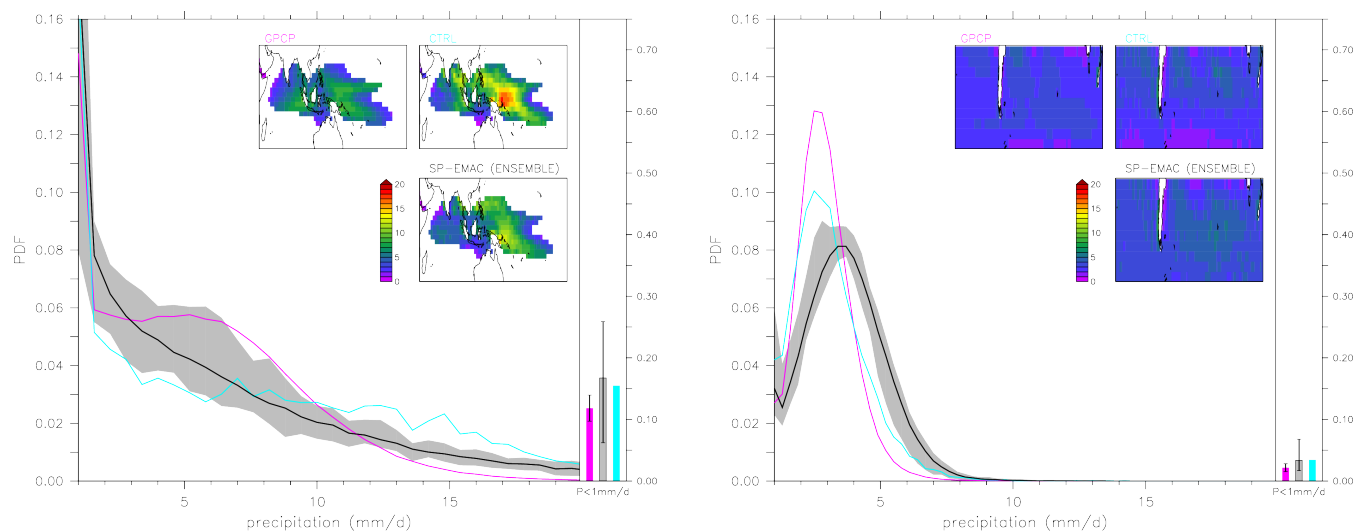
Figure 5. PDFs of monthly precipitation rates for the Warm Pool region and southern ocean mid-latitudes comparing to 30-years of GPCP data (same as in table 2). Maps show yearly averaged rates for the specified region in mm/d. On the right hand sight of each figure the fraction of non-precipitating cells (below 1 mm/d) is displayed including the interannual variability for the GPCP data and the variability induced by different SP-EMAC configurations (uncertainty bars). Note: x-axis begins at 1 mm/d.

(Wang et al., 2011a). Regardless of these studies, SP-EMAC sensitivity runs suggest that formation of precipitation including the ice phase (or mixed-phase) is substantially better simulated than rainfall in almost pure liquid clouds that is often the case for maritime precipitation in the southern mid-latitudes (Matsui et al., 2016). Nevertheless, a high sensitivity in precipitation is visible within the ITCZ and the northern and southern mid-latitudes depending on the CRM configuration. Analysing this

5 in more detail it emerges that the contribution of this variability is mostly generated above the oceans and coastal regions (not shown). That implies that simulated precipitation rates are sensitive to land-ocean contrasts.

Focusing on two specific regions figure 5 displays probability density functions of monthly precipitation rates for the Warm Pool Region and the southern ocean mid-latitudes. The former is defined as an area where sea surface temperatures exceed 297 K and strong convective systems develop whereas the latter defines only oceanic regions in the southern hemisphere

10 between 36° and 64° characteristically associated with marine boundary layer clouds (Mace, 2010; Haynes et al., 2011). Embedded maps present the spatial distribution for the chosen region as yearly averaged precipitation rates. In addition to that the non-precipitating fraction (below 1 mm/d) is shown as bars including the variability of SP-EMAC induced when choosing different configurations and the interannual variability of the observational data. Based on the overall improvement for SP-EMAC to simulate precipitation in the Warm Pool region the PDF shows important characteristics that are to some extent

15 reproduced by the superparametrisation. The most distinct feature for the maritime continent PDF is the high variability for the SP-EMAC simulations covering almost the entire range of observed probabilities. Compared to the control simulation it is most obvious that high precipitation rates (above 10 mm/d) are better represented by the CRM. Precipitation rates between 3 and 10 mm/d are underestimated by almost all simulations. Depending on the chosen configuration it can be concluded that

the configurations OR1 4km 64, OR1 2km 64, OR2 4km 64 and OR2 2km 64 produce the best estimate of precipitation in the Warm Pool region. Each of these simulations show enhanced precipitation probabilities between 5 to 10 mm/d and produce the lowest probabilities for high precipitation rates in agreement with the GPCP observations (not shown). Comparing the spatial distributions a single maximum precipitation spot is visible in the western pacific when using the convection parametrisation.

5 This is not as prominent for the SP-EMAC simulations displaying a more widespread distribution. At last non-precipitation probabilities (comparing boxes at the right side of the plot) are in close agreement with the GPCP data but expose a huge variability for SP-EMAC reflecting the strong dependence on the chosen configuration.

The comparison of precipitation rates in the southern hemisphere mid-latitudes reveals two systematic problems of SP-EMAC: an underestimation of lower precipitation rates (between 1 to 5 mm/d) and a shift in peak precipitation rate from the ob-

10 served value of 2.5 mm/d to almost 4 mm/d explaining the overestimation in figure 3. This feature is significant for all superparametrised simulations independent of the chosen CRM configuration. Furthermore the comparison of almost non-precipitating grid cells reveals a similar amount of dry days in comparison with the control simulation. This finding is in agreement with other models showing a similar behaviour between parametrised and superparametrised simulations (see Kooperman et al., 2016, supplement S2). All in all the control simulation can reproduce the peak precipitation whereas it is skewed

15 to larger values (above 4 mm/d). Pointing out the differences in the microphysics one has to consider the different autoconversion rates used within the CRM cells and within the cloud scheme of the control run. The superparametrisation uses a simple fixed conversion rate (see Khairoutdinov and Randall, 2003, Appendix D) whereas the cloud scheme uses the formulation of Beheng (1994). Focusing on this aspect Suzuki et al. (2015) has shown that the distribution of precipitation categories (non-precipitating, drizzle, rain) is dependent on its expression thereby influencing the precipitation rate. Future studies with

20 SP-EMAC should investigate the onset of precipitation for maritime clouds in more detail or should consider using a two-moment microphysical scheme and its coupling to an aerosol submodel.

Apart from the distribution of precipitation a known problem of GCMs is the incorrect representation of the diurnal cycle in precipitation within the tropics (Collier and Bowman, 2004; Dai, 2006). Improvements have been suggested by Bechtold et al. (2004) for convection parametrisations based on their entrainment rates. Additionally, superparametrised GCMs have been

25 studied and show progress in representing the diurnal cycle of precipitation and its contrast between ocean and land (Khairoutdinov et al., 2005; Zhang et al., 2008; Pritchard and Somerville, 2009a, b; Tao et al., 2009). In order to analyse this process the output has been increased to produce precipitation rates on a hourly basis for one entire month (July). Instead of using the full SP-EMAC ensemble only a subset of superparametrised simulations with an annual precipitation below 3 mm/d has been chosen. These simulations have been selected because they have the smallest difference in comparison to observational

30 data (compare with table 2). The hourly output has been compared to multi-monthly July averages of TRMM data between 1998 and 2010. Figure 6 displays the averaged diurnal precipitation transformed to local solar time for continental and oceanic grid points between 30° latitudes around the equator. Investigating the diurnal precipitation over land observational evidence exposes a peak around 17 LT and an onset in precipitation around 9 LT. The control simulation does not reproduce any of these timings confirming the difficulty of GCMs including convection parametrisations to correctly simulate the diurnal cycle. The

35 onset and peak of precipitation is around 3 hours too early and the amplitude is overestimated. Many aspects of this evolution
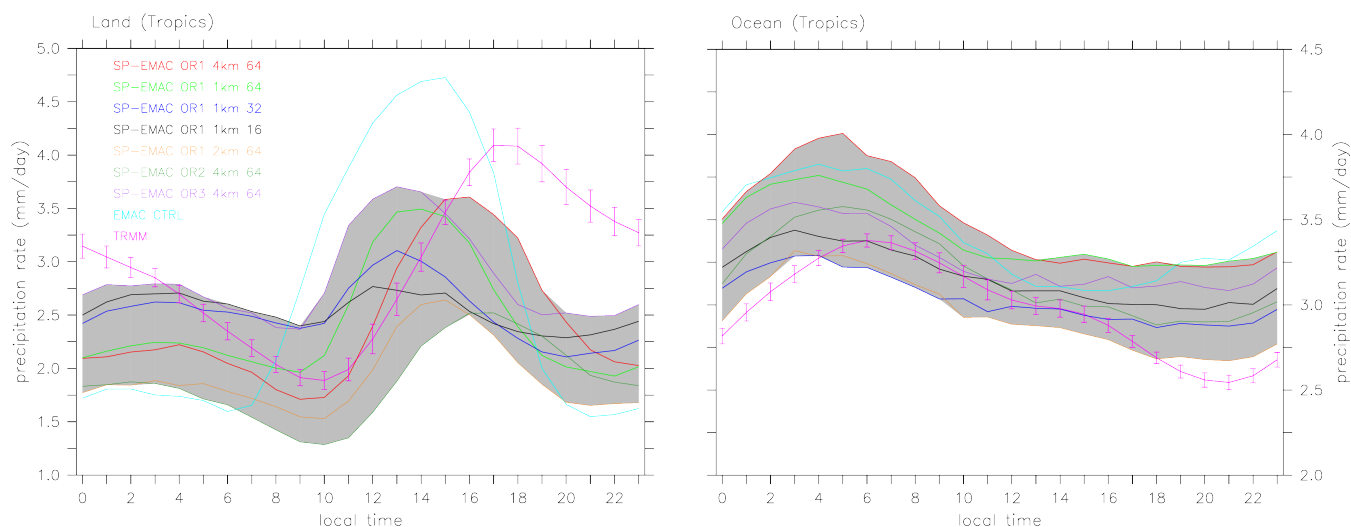
Figure 6. Comparison of diurnal tropical precipitation (30° around the equator) for land and ocean with 3-hourly TRMM data* between 1998 and 2010 for the month July. The observational standard deviation is shown by error bars indicating interannual variability in the diurnal cycle. The grey area covers the variability of all SP-EMAC configurations.

* Tropical Rainfall Measuring Mission (TRMM) (2011), TRMM (TMPA) Rainfall Estimate, L3, 3 hour, 0.25°x0.25°, V7, Greenbelt, MD, Goddard Earth Sciences Data and Information Services Center (GES DISC), Accessed: 02/11/2018, DOI: http://doi.org/10.5067/TRMM/ TMPA/3H/7, Huffman et al. (2007)

can be attributed to diminishing CIN (convecitve inhibition) during sunrise and increasing CAPE (convective available poten-
tial energy) during the day that are the basis of triggering and sustaining the convection parametrisation. The shift of a too early
precipitation onset is substantially improved using any kind of SP-EMAC simulation. Independent of the CRM configuration
the timing of the onset of precipitation is almost perfectly reflected in comparison to TRMM data. This indicates that cloud
5 evolution is not only coupled to the diurnal solar insolation but follows PBL evolution. In contrast diurnal peak precipitation
is completely dependent on the CRM configuration for SP-EMAC indicating values between 2.5 to 3.75 mm/d and peak time
spreading from 12 LT (OR1 1km 16) to 17 LT (OR2 4km 64). Furthermore the decline in precipitation after peaking is too
strong resulting in a secondary maximum during the night (between 2 to 5 LT). This secondary peak is partly visible for the
TRMM data but only for spring and autumn seasons (Yang and Smith, 2006). Even if the diurnal cycle is not captured very well
10 it has almost no influence on the global mean precipitation rate. One significant highlight corresponds to the different diurnal
amplitudes, which increase with increasing number of CRM cells, whereas single simulations with 32 or 16 cells exhibit a
small or almost no diurnal cycle in precipitation.

The diurnal cycle over tropical oceans is displayed on the right side in figure 6. The observed diurnal cycle presents a peak
in precipitation around 6 LT and a clear minimum in the evening hours (21 LT). A saddle point (secondary maximum) can
15 be identified around 14 LT. The primary mechanisms to explain this cycle are: „static radiation-convection" and „dynamic
radiation-convection" that describes the process of radiative cooling while increasing thermodynamic instability enhancing

nighttime precipitation or suppressing daytime rainfall through decreased convergence into the convective region. A more detailed description and further mechanisms are given in Yang and Smith (2006).

The control simulation shows an overall overestimation of oceanic precipitation rates by 0.5 mm/d but a similar timing in peak precipitation. The simulated decline in oceanic rainfall is too steep resulting in too early minimum precipitation rate around

5   15 LT and an increase directly afterwards. In contrast nearly all SP-EMAC runs simulate a consistent decline as CTRL after peaking precipitation between 4 and 6 LT but remain almost constant until 21 LT. The spread in oceanic precipitation rates of the SP-EMAC ensemble is slightly lower (0.75 mm/d) compared to the diurnal cycle over land (1.25 mm/d). Analogous to the diurnal cycle over land it emerges that the amplitude of precipitation rates increases with an increasing number of CRM cells. Especially two specific configurations (OR1 2km 64 and OR2 4mk 64) are in very good agreement with TRMM data. Never-

10 theless all simulations miss the representation of a secondary maximum around 14 LT. This effect could be due to neglected diurnal variations in prescribed SSTs thereby restraining ocean surface heating (Sui et al., 1997, 1998). Further investigations of 2D cloud-resolving model simulations with diurnally varying SSTs exhibit an increase in afternoon rain rates suggesting influences of ocean heating in atmospheric moistening and drying throughout the day (Cui and Li, 2009).

To complete the regional analysis of SP-EMAC cloud radiative effects at the top of the atmosphere are investigated. Ten years

15 of satellite data of CERES are used for comparison (see table 2). CRE is divided into its longwave and shortwave component to distinguish different radiative effects. Zonal averages of cloud radiative effects are shown in figure 7. Instead of displaying all individual SP-EMAC simulations the ensemble mean (black lines) and spread (grey area) is shown. The distribution of NetCRE shows high discrepancies in the mid-latitudes. The primary cause of this difference is induced by the shortwave component of the CRE revealing the representation of too reflective clouds in all simulations for this region. Moreover, seasonal variation for

20 CRE_{SW} are enhanced in all SP-EMAC simulations as well as in the control run. Smaller deviations for NetCRE are visible in the ITCZ for SP-EMAC compensated by even larger differences for the individual components CRE_{SW} and CRE_{LW}. Comparing CTRL and SP-EMAC in a comprehensive sense it emerges that overall CTRL represents the zonal NetCRE distribution slightly better especially in the Tropics. This is sometimes due to compensating errors. On a closer look many SP-EMAC configurations improve the longwave and shortwave component in the mid-latitudes. Nevertheless dependent on the CRM

25 configuration there exists high differences even in the zonal mean distribution. To identify regions with significant differences figure 8 shows absolute differences of NetCRE, CRE_{SW} and CRE_{LW}. Similar t-Tests as for figure 4 have been performed to obtain important areas that deviate from CERES observations. Thereby non-significant differences are shown in white. Blue areas indicate regions where cloud radiative effects are stronger (higher cooling) whereas red areas specify less cooling or even a warming effect of clouds. Comparing the differences in NetCRE maps in figure 8 it is apparent that CTRL show larger areas

30 of significant differences especially a positive bias over the oceans. The underestimation of cloud radiative effects for CTRL over the oceans is because of a much higher shortwave component in these regions marking a reduced amount in low cloud cover or less reflective clouds in the areas of stratocumulus decks. Using a superparametrisation in EMAC results in smaller discrepancies for all CRE components. In particular the formerly mentioned regions demonstrate a better representation of radiative effects of low clouds. However a significant reduction of about 10 W/m² to 20 W/m² is visible for the Western Pacific

35 region in many SP-EMAC simulations. Evaluating the longwave and shortwave component in these region it became apparent
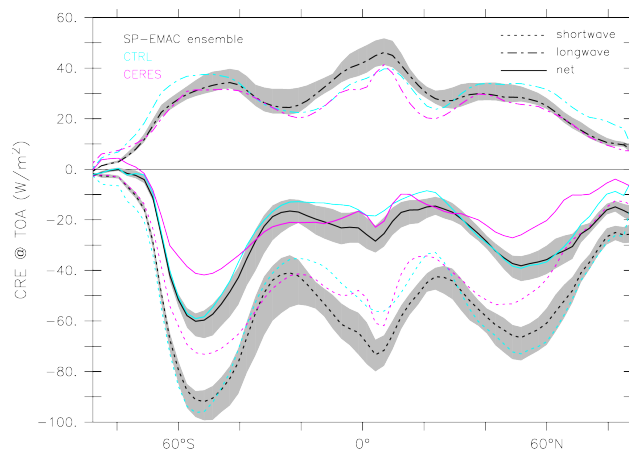
Figure 7. Zonal averaged simulated top-of-atmosphere cloud-radiative effects (CRE) compared to CERES EBAF-TOA data (2000-2010).

that deep convective clouds have an increased optical depth for many CRM configurations and concurrently a higher liquid and ice water content than the control simulation (not shown). Further important differences are visible for CRE_{LW} in the control simulation. A stronger warming over the complete southern ocean and the arctic region is apparent as a result of a too high liquid water path in these regions. Lastly, comparing all maps from top to bottom in figure 8, it is possible to easily identify

5 regions that show almost no significant difference in NetCRE because of compensating errors in the longwave and shortwave part. Affected areas are: Central Africa, Central America and the Caribbean Sea for SP-EMAC and the Sahara, Greenland, North America, the Arctic and the Southern Ocean for CTRL. Thereby it is evident that NetCRE should not be used as a single metric to evaluate cloud radiative effects and the performance of a GCM. All in all, CRE is influenced by multiple factors: insolation, cloud amount, cloud type and surface properties (albedo). Only cloud amount and cloud type changes are relevant

10 for explaining differences between SP-EMAC and CTRL (excluding glaciers and snow-covered areas that increase surface albedo). Even if SP-EMAC seems to reduce CRE errors, different configurations show significant different results. Therefore it is not appropriate to use any CRM configuration as a superparametrisation in EMAC.

3.3 Issues due to CRM's configuration

15 The global evaluation of SP-EMAC in chapter 3.1 has revealed some major influences of the CRM configuration onto the mean climate state. Summarizing table 2 it can be shown that all SP-EMAC simulations can be split into two ensemble subsets depending on their mean land surface temperature and precipitation rate. Simulations with a maximum surface temperature of 290 K and precipitation rate below 3.0 mm/d are referred to sub-ensemble A whereas all other simulations ($T_s > 290$ K; $P < 3.0$ mm/d) characterise sub-ensemble B. Based upon the global mean Taylor diagrams in figure 2 no clear separation of

20 SP-EMAC simulations in two branches is noticeable. Tracking down other differences than mean surface temperatures and precipitation rates among SP-EMAC simulations the distribution of surface heat fluxes is observed. Figure 9 shows the Taylor

diagram of sensible and latent heat flux over land and its mean zonal distribution. The fluxes are compared to NCEP reanalysis data (compare with table 2) between 1979 and 2010. Evaluating the Taylor diagram it is clearly visible that heat fluxes are rapidly degraded for sub-ensemble B. Especially latent heat fluxes are strongly influenced displaying a very low correlation and standard deviation compared to the reanalysis data. This deterioration is a clear consequence of lower precipitation rates

5 over land inducing stronger surface temperature changes. The latter stabilize the temperature gradient of the troposphere creating a positive feedback in reducing the probability of deep convective clouds with heavy precipitation. The zonal distribution in figure 9 emphasize a significant global reduction of the latent heat flux for sub-ensemble B and an overestimation of the sensible heat flux. Additionally, a very similar distribution in comparison with observations is depicted by sub-ensemble A with slightly improved correlations for both heat fluxes comparing to CTRL. The analysis of heat fluxes clearly shows that

10 a changing configuration of the superparametrisation impacts lower tropospheric properties on a global scale representing a different kind of climate state. Focusing on sub-ensemble B and its specific configurations it is interesting to notice that mainly OR2 and OR3 orientations (north-south orientation and 3D CRM) with CRM grid spacing mostly below 4 km are included in this subset. This could indicate that the directional wind speed has an impact on the simulated fields and further suggestions like allowing 2D-CRM orientations to vary with time could avoid this problem (Cheng and Xu, 2014; Jung and Arakawa, 2016).

15 Especially only one three-dimensional setup (OR3 4km 64) and one two-dimensional (OR2 4km 64) setup illustrate a climate state with T_s above 290 K and P below 3.0 mm/d suggesting that all other 3D-CRM (or 2D north-to-south oriented) setups are too small to realistically represent correct lower troposphere features. Nonetheless heat fluxes are not the only aspect of the sub-ensembles that differ significantly. Because precipitation rates show a small indication of dividing the SP-EMAC simulations into two branches it is straightforward to observe cloud related variables. Therefore cloud optical thickness (COT) for

20 continental clouds is examined using satellite data from the Moderate Resolution Imaging Spectroradiometer (MODIS) collection 5.1. Observation between 2003 and 2015 from the combined Terra and Aqua satellites are remapped onto the coarse GCM grid and used for comparison purposes. Figure 10 shows the Taylor diagram and zonal distribution of cloud optical thickness. Similar to the heat fluxes the Taylor diagram for cloud optical thickness clearly separates all simulations of sub-ensemble A from sub-ensemble B. Apart from that, a better performance is indicated for the latter one because of a reduced standard devi-

25 ation. The zonal distribution clarifies the improved representation for sub-ensemble B by a decline in optical thickness within the ITCZ. Generally speaking all SP-EMAC simulations display a similar distribution as CTRL in the mid-latitudes whereas tropical cloud thicknesses over land are overestimated. This increase in COT partly explains the stronger cloud radiative effects for all SP-EMAC runs compensating the overall reduced simulated cloud amount. However, the comparison with MODIS data shows a strongly reduced correlation.

30 In summary, it has been shown that different configurations of the CRM within SP-EMAC lead to distinctive atmospheric properties demonstrated by diverse heat fluxes and cloud optical depths. These results suggest that cloud evolution and processing within the superparametrisation is influenced because of different domain compositions. Even if all members of sub-ensemble A show a better performance than sub-ensemble B in terms of climate metrics it should be noted that further tuning is necessary. In particular it is necessary to adjust cloud amount and cloud optical properties. This would further improve the

simulation of cloud-radiative effects and reduce the compensation of contrarily effects.

4   Conclusions and Discussion

The concept of embedding a cloud-resolving model into a GCM has been studied for over a decade and this paper introduce
another climate model incorporating this idea. The superparametrisation based upon the System for Atmospheric Modeling
(SAM, Khairoutdinov et al. (2008)) has been included into the EMAC model. This study focused on the effect of different
model configurations of the embedded CRM (orientation, cell size, number of cells) on climate relevant variables. For the first
time the influence of different aspects of the superparametrisation has been systematically evaluated in 20 model simulations
each spanning one year. The model runs have been compared to observations and a control simulation using a conventional
convection parametrisation and a large-scale cloud microphysics scheme.

The analysis of global mean statistics for all superparametrised runs encompassing the net radiative flux at TOA, surface tem-
perature, cloud amount, precipitation, LWP, IWP and the net cloud radiative effect show similar results compared to the control
simulation. Almost all global mean results lie within the range of CMIP5 models independent of the chosen CRM configura-
tion. Only three superparametrised setups covering a relatively small area within the GCM grid box and a three dimensional
CRM orientation simulate a high energy imbalance. This supports the assumption that a minimum CRM ensemble size is
necessary to represent cloud development covering all important subgrid-scales of a GCM. Taylor diagrams reveal improved
representations of the longwave radiative flux at TOA, cloud cover distribution and a similar distribution of atmospheric humid-
ity using a superparametrisation in EMAC. The global distribution of precipitation rates show a degradation when comparing to
GPCP data because of a too high oceanic rainfall but a better performance for the Warm Pool region. Interestingly, a rather high
influence depending on the selected CRM configuration is evident concerning precipitating fields especially over the western
Pacific. Related to the analysis of rainfall PDFs the amount of non-precipitating grid cells (below 1 mm/d) is highly variable
indicating contrasting onsets in precipitation for different CRM configurations for the Warm Pool and southern hemisphere
mid-latitude region.

Furthermore the diurnal cycle for tropical land and oceans has been observed separately. Independent of the configuration of
the superparametrisation the onset of tropical precipitation over land is in perfect agreement with TRMM data as contrasted
with the control simulation. Nevertheless, the configuration of the CRM drastically changes the amplitude and peak in precip-
itation in the tropics. Thereby some model setups of the superparametrisation show similar precipitation peaks in the diurnal
cycle as compared to the control simulation using a convection parametrisation with even diminishing amplitudes. This con-
clusion stands in contrast with recent literature proclaiming a great improvement in the simulation of the diurnal cycle using
any kind of superparametrisation. A rather significant feature throughout the simulations is the decreasing diurnal amplitude
when defining smaller sets of CRM cells for the superparametrised setup.

Regarding the cloud-radiation interaction it appears that the control simulation shows a slightly better representation of the
net cloud radiative effect comparing the zonal distribution. However a regional analysis demonstrates that larger areas display

significant differences in CRE contrasting the control simulation with the superparametrised runs. In comparison with CERES satellite data and the distribution of the longwave and shortwave CRE it is evident that many regions show opposing effects resulting in compensating errors in the NetCRE. Many setups of the superparametrisation show improvements especially over oceanic regions for CRE_{LW} and CRE_{SW} but this can not be stated for any kind of CRM setup.

5   A major consideration in this study has been the issues associated with changes in CRM orientation, size or the numbers of small-scale grid cells. It has been shown that global lower tropospheric features in particular surface heat fluxes are primarily influenced when changing CRM aspects representing different kind of climate states. These differences are mainly induced by feedback mechanisms through perturbations of precipitation efficiency, atmospheric stability and surface properties. Thereby a smaller but still similar impact is visible regarding cloud optical thickness over land. These dependencies are important to

10   characterize for further EMAC model simulations using a similar kind of CRM setups. The usage of superparametrised GCMs is still highly computational expensive (factor 15 to 45 increase in CPU time using 16 to 64 cells in a 2D orientation; factor 40 to 120 using the full 3D setup with 16 to 64 cells for EMAC simulations) and it is thereby desirable to use as few as possible resources without significantly modifying the model performance. For the superparametrised EMAC it has been shown that using the north-south oriented CRM it is necessary to have at least 64 cells with a 4 km cell size to obtain similar metrics

15   as the control simulation. The same result is obtained for the 3D configuration. The east-west configuration shows a lower sensitivity when using a different kind of setup suggesting that an ensemble of 64 cells provide enough variability to reproduce a realistic mean statistical subgrid-scale feedback for CRM grid cell sizes between 1 and 4 km. All in all, it is therefore recommended to use 64 cells for any setup of the superparametrisation. Furthermore, based on the performed analysis it is assumed that increasing the GCMs resolution to grid spacing between 50 to 100 km and successively adapting the CRM domain could

20   lead to unexpected results because CRM ensemble statistics influence the mean climate state. In particular it seems that cloud evolution inside of the CRM is prevented using 32 or less cells thereby it is necessary to establish the communication across GCM cells (Arakawa et al., 2011; Jung and Arakawa, 2010).

In conclusion, a last point has to be taken into account that deals with the almost neglected tuning process of the super-parametrised version of EMAC. In order to optimise a GCM thousands of model runs are required to cover the complete

25   parametric space of tunable variables. In addition to that, multiple process- or target-oriented constraints should be used to achieve a best model estimate for present-day climatology (Hourdin et al., 2017). Within this study the only limitation has been the energy balance at the top of the atmosphere. Future studies should for the time being focus on tuning this version of EMAC to multiple observational data sets especially aiming attention at cloud amounts. Because of the high computational expense it would be advantageous to use shorter hindcast simulations with an automatic tuning in order to accelerate the progress of the

30   superparametrised version of EMAC (Zhang et al., 2018).

The modular framework of MESSy provides an optimal model structure to easily couple the superparametrisation with other submodels. First steps has been taken to adapt cloud optical calculations and the radiative transfer scheme to be applied with subgrid-scale outputs of the CRM. Other future studies should deal with transporting chemical tracers within the super-parametrisation. This would give new insights when evaluating the subgrid-scale transport of various trace gases and their

diverse atmospheric lifetimes in comparison to GCM transport routines using parametrised massfluxes to describe the vertical transport.

Code availability. The Modular Earth Submodel System (MESSy) is continuously further developed and applied by a consortium of institutions. The usage of MESSy and access to the source code is licensed to all affiliates of institutions which are members of the MESSy

5 Consortium. Institutions can become a member of the MESSy Consortium by signing the MESSy Memorandum of Understanding. More information can be found on the MESSy Consortium Website (www.messy-interface.org). As the MESSy code is only available under license, no DOI is possible for MESSy code versions.

The code for using the superparametrised version of EMAC used in this manuscript will be included in the next official MESSy version (v2.55).

10 *Data availability.* All presented datasets are freely available. If possible DOIs or corresponding websites have been issued containing a brief summary of the corresponding dataset and a link to the data access page.

Author contributions. HR and HT designed the experiments. HR implemented the model code, performed the simulations and analysed the data. HR wrote the manuscript with support from HT. HT supervised the project.

Competing interests. The authors declare that they have no conflict of interest.

15 *Acknowledgements.* Parts of this research were conducted using the supercomputer Mogon and/or advisory services offered by Johannes Gutenberg University Mainz (https://hpc.uni-mainz.de), which is a member of the AHRP (Alliance for High Performance Computing in Rhineland Palatinate, www.ahrp.info) and the Gauss Alliance e.V. The authors gratefully acknowledge the computing time granted on the supercomputer Mogon at Johannes Gutenberg University Mainz.

References

Adler, R., Sapiano, M., Huffman, G., Wang, J., Gu, G., Bolvin, D., Chiu, L., Schneider, U., Becker, A., Nelkin, E., Xie, P., Ferraro, R., and Shin, D.: The Global Precipitation Climatology Project (GPCP) monthly analysis (New Version 2.3) and a review of 2017 global precipitation, Atmosphere, 9, https://doi.org/10.3390/atmos9040138, 2018.

5   Arakawa, A., Jung, J. H., and Wu, C. M.: Toward unification of the multiscale modeling of the atmosphere, Atmospheric Chemistry and Physics, 11, 3731–3742, https://doi.org/10.5194/acp-11-3731-2011, 2011.

Baumgaertner, A. J. G., Joeckel, P., Kerkweg, A., Sander, R., and Tost, H.: Implementation of the Community Earth System Model (CESM) version 1.2.1 as a new base model into version 2.50 of the MESSy framework, Geosci. Model Dev., 9, 125–135, http://www.geosci-model-dev.net/9/125/2016/, 2016.

10   Bechtold, P., Chaboureau, J. P., Beljaars, A., Betts, A. K., Kohler, M., Miller, M., and Redelsperger, J. L.: The simulation of the diurnal cycle of convective precipitation over land in a global model, Quarterly Journal of the Royal Meteorological Society, 130, 3119–3137, 2004.

Beheng, K.: A parameterization of warm cloud microphysical conversion processes, Atmospheric Research, 33, 193 – 206, https://doi.org/10.1016/0169-8095(94)90020-5, 11th International Conference on Clouds and Precipitation, Part II, 1994.

Boucher, O., Randall, D., Artaxo, P., Bretherton, C., Feingold, G., Forster, P., Kerminen, V.-M., Kondo, Y., Liao, H., Lohmann, U., Rasch, P.,

15   Satheesh, S., Sherwood, S., Stevens, B., and Zhang, X.: Clouds and Aerosols, book section 7, pp. 571–658, Cambridge University Press, Cambridge, United Kingdom and New York, NY, USA, https://doi.org/10.1017/CBO9781107415324.016, www.climatechange2013.org, 2013.

Calisto, M., Folini, D., Wild, M., and Bengtsson, L.: Cloud radiative forcing intercomparison between fully coupled CMIP5 models and CERES satellite data, Annales Geophysicae, 32, 793–807, https://doi.org/10.5194/angeo-32-793-2014, 2014.

20   Cheng, A. and Xu, K.-M.: An explicit representation of vertical momentum transport in a multiscale modeling framework through its 2-D cloud-resolving model component, Journal of Geophysical Research: Atmospheres, 119, 2356–2374, https://doi.org/10.1002/2013JD021078, 2014.

Cheng, A. N. and Xu, K. M.: Diurnal variability of low clouds in the Southeast Pacific simulated by a multiscale modeling framework model, Journal of Geophysical Research: Atmospheres, 118, 9191–9208, https://doi.org/10.1002/jgrd.50683, 2013.

25   Cole, J. N. S., Barker, H. W., Randall, D. A., Khairoutdinov, M. F., and Clothiaux, E. E.: Global consequences of interactions between clouds and radiation at scales unresolved by global climate models, Geophysical Research Letters, 32, L06 703, https://doi.org/10.1029/2004GL020945, 2005.

Collier, J. C. and Bowman, K. P.: Diurnal cycle of tropical precipitation in a general circulation model, Journal of Geophysical Research: Atmospheres, 109, https://doi.org/10.1029/2004JD004818, d17105, 2004.

30   Cui, X. and Li, X.: Diurnal responses of tropical convective and stratiform rainfall to diurnally varying sea surface temperature, Meteorology and Atmospheric Physics, 104, 53–61, https://doi.org/10.1007/s00703-008-0016-1, 2009.

Dai, A.: Precipitation Characteristics in Eighteen Coupled Climate Models, Journal of Climate, 19, 4605–4630, https://doi.org/10.1175/JCLI3884.1, 2006.

Dietmüller, S., Jöckel, P., Tost, H., Kunze, M., Gellhorn, C., Brinkop, S., Frömming, C., Ponater, M., Steil, B., Lauer, A., and Hendricks, J.: A

35   new radiation infrastructure for the Modular Earth Submodel System (MESSy, based on version 2.51), Geoscientific Model Development, 9, 2209–2222, https://doi.org/10.5194/gmd-9-2209-2016, 2016.

Eyring, V., Bony, S., Meehl, G. A., Senior, C. A., Stevens, B., Stouffer, R. J., and Taylor, K. E.: Overview of the Coupled Model Intercomparison Project Phase 6 (CMIP6) experimental design and organization, Geoscientific Model Development, 9, 1937–1958, https://doi.org/10.5194/gmd-9-1937-2016, 2016.

Flato, G., Marotzke, J., Abiodun, B., Braconnot, P., Chou, S., Collins, W., Cox, P., Driouech, F., Emori, S., Eyring, V., Forest, C., Gleckler, P., Guilyardi, E., Jakob, C., Kattsov, V., Reason, C., and Rummukainen, M.: Evaluation of Climate Models, book section 9, p. 741–866, Cambridge University Press, Cambridge, United Kingdom and New York, NY, USA, https://doi.org/10.1017/CBO9781107415324.020, www.climatechange2013.org, 2013.

Grabowski, W. W.: Coupling cloud processes with the large-scale dynamics using the Cloud-Resolving Convection Parameterization (CRCP), Journal of the Atmospheric Sciences, 58, 978–997, https://doi.org/10.1175/1520-0469(2001)058<0978:CCPWTL>2.0.CO;2, 2001.

Grabowski, W. W. and Smolarkiewicz, P. K.: CRCP: a Cloud Resolving Convection Parameterization for modeling the tropical convecting atmosphere, Physica D, 133, 171–178, https://doi.org/10.1016/S0167-2789(99)00104-9, 1999.

Gustafson, W. I., Berg, L. K., Easter, R. C., and Ghan, S. J.: The Explicit-Cloud Parameterized-Pollutant hybrid approach for aerosol-cloud interactions in multiscale modeling framework models: tracer transport results, Environmental Research Letters, 3, 025 005, 2008.

Haarsma, R. J., Roberts, M. J., Vidale, P. L., Senior, C. A., Bellucci, A., Bao, Q., Chang, P., Corti, S., Fučkar, N. S., Guemas, V., von Hardenberg, J., Hazeleger, W., Kodama, C., Koenigk, T., Leung, L. R., Lu, J., Luo, J.-J., Mao, J., Mizielinski, M. S., Mizuta, R., Nobre, P., Satoh, M., Scoccimarro, E., Semmler, T., Small, J., and von Storch, J.-S.: High Resolution Model Intercomparison Project (HighResMIP v1.0) for CMIP6, Geoscientific Model Development, 9, 4185–4208, https://doi.org/10.5194/gmd-9-4185-2016, 2016.

Haynes, J. M., Jakob, C., Rossow, W. B., Tselioudis, G., and Brown, J.: Major Characteristics of Southern Ocean Cloud Regimes and Their Effects on the Energy Budget, Journal of Climate, 24, 5061–5080, https://doi.org/10.1175/2011JCLI4052.1, 2011.

Heinze, R., Dipankar, A., Henken, C. C., Moseley, C., Sourdeval, O., Trömel, S., Xie, X., Adamidis, P., Ament, F., Baars, H., Barthlott, C., Behrendt, A., Blahak, U., Bley, S., Brdar, S., Brueck, M., Crewell, S., Deneke, H., Di Girolamo, P., Evaristo, R., Fischer, J., Frank, C., Friederichs, P., Göcke, T., Gorges, K., Hande, L., Hanke, M., Hansen, A., Hege, H.-C., Hoose, C., Jahns, T., Kalthoff, N., Klocke, D., Kneifel, S., Knippertz, P., Kuhn, A., van Laar, T., Macke, A., Maurer, V., Mayer, B., Meyer, C. I., Muppa, S. K., Neggers, R. A. J., Orlandi, E., Pantillon, F., Pospichal, B., Röber, N., Scheck, L., Seifert, A., Seifert, P., Senf, F., Siligam, P., Simmer, C., Steinke, S., Stevens, B., Wapler, K., Weniger, M., Wulfmeyer, V., Zängl, G., Zhang, D., and Quaas, J.: Large-eddy simulations over Germany using ICON: a comprehensive evaluation, Quarterly Journal of the Royal Meteorological Society, 143, 69–100, https://doi.org/10.1002/qj.2947, 2017.

Hourdin, F., Mauritsen, T., Gettelman, A., Golaz, J.-C., Balaji, V., Duan, Q., Folini, D., Ji, D., Klocke, D., Qian, Y., Rauser, F., Rio, C., Tomassini, L., Watanabe, M., and Williamson, D.: The Art and Science of Climate Model Tuning, Bulletin of the American Meteorological Society, 98, 589–602, https://doi.org/10.1175/BAMS-D-15-00135.1, 2017.

Huffman, G. J., Bolvin, D. T., Nelkin, E. J., Wolff, D. B., Adler, R. F., Gu, G., Hong, Y., Bowman, K. P., and Stocker, E. F.: The TRMM Multisatellite Precipitation Analysis (TMPA): Quasi-Global, Multiyear, Combined-Sensor Precipitation Estimates at Fine Scales, Journal of Hydrometeorology, 8, 38–55, https://doi.org/10.1175/JHM560.1, 2007.

Jiang, J. H., Su, H., Zhai, C. X., Perun, V. S., Del Genio, A., Nazarenko, L. S., Donner, L. J., Horowitz, L., Seman, C., Cole, J., Gettelman, A., Ringer, M. A., Rotstayn, L., Jeffrey, S., Wu, T. W., Brient, F., Dufresne, J. L., Kawai, H., Koshiro, T., Watanabe, M., LEcuyer, T. S., Volodin, E. M., Iversen, T., Drange, H., Mesquita, M. D. S., Read, W. G., Waters, J. W., Tian, B. J., Teixeira, J., and Stephens, G. L.: Evaluation of cloud and water vapor simulations in CMIP5 climate models using NASA "A-Train" satellite observations, Journal of Geophysical Research-atmospheres, 117, D14 105, https://doi.org/10.1029/2011JD017237, 2012.

Joeckel, P., Sander, R., Kerkweg, A., Tost, H., and Lelieveld, J.: Technical Note: The Modular Earth Submodel System (MESSy) - A new approach towards Earth System Modeling, Atmospheric Chemistry and Physics, 5, 433–444, https://doi.org/10.5194/acp-5-433-2005, 2005.

Joeckel, P., Kerkweg, A., Pozzer, A., Sander, R., Tost, H., Riede, H., Baumgaertner, A., Gromov, S., and Kern, B.: Development cycle 2 of the Modular Earth Submodel System (MESSy2), Geoscientific Model Development, 3, 717–752, https://doi.org/10.5194/gmd-3-717-2010, 2010.

Jung, J. H. and Arakawa, A.: Development of a Quasi-3D Multiscale Modeling Framework: Motivation, Basic Algorithm and Preliminary results, Journal of Advances In Modeling Earth Systems, 2, 11, https://doi.org/10.3894/JAMES.2010.2.11, 2010.

Jung, J. H. and Arakawa, A.: Simulation of subgrid orographic precipitation with an embedded 2-D cloud-resolving model, Journal of Advances In Modeling Earth Systems, 8, 31–40, https://doi.org/10.1002/2015MS000539, 2016.

Kajikawa, Y., Miyamoto, Y., Yoshida, R., Yamaura, T., Yashiro, H., and Tomita, H.: Resolution dependence of deep convections in a global simulation from over 10-kilometer to sub-kilometer grid spacing, Progress in Earth and Planetary Science, 3, 16, https://doi.org/10.1186/s40645-016-0094-5, 2016.

Kajikawa, Y., Yamaura, T., Tomita, H., and Satoh, M.: Impact of Tropical Disturbance on the Indian Summer Monsoon Onset Simulated by a Global Cloud-System-Resolving Model, SOLA, 11, 80–84, https://doi.org/10.2151/sola.2015-020, 2015.

Kanamitsu, M., Ebisuzaki, W., Woollen, J., Yang, S.-K., Hnilo, J. J., Fiorino, M., and Potter, G. L.: NCEP–DOE AMIP-II Reanalysis (R-2), Bulletin of the American Meteorological Society, 83, 1631–1643, https://doi.org/10.1175/BAMS-83-11-1631, 2002.

Karlsson, K.-G., Anttila, K., Trentmann, J., Stengel, M., Fokke Meirink, J., Devasthale, A., Hanschmann, T., Kothe, S., Jääskeläinen, E., Sedlar, J., Benas, N., van Zadelhoff, G.-J., Schlundt, C., Stein, D., Finkensieper, S., Håkansson, N., and Hollmann, R.: CLARA-A2: the second edition of the CM SAF cloud and radiation data record from 34 years of global AVHRR data, Atmos. Chem. Phys., 17, 5809–5828, https://www.atmos-chem-phys.net/17/5809/2017/, 2017.

Kerkweg, A. and Jöckel, P.: The 1-way on-line coupled atmospheric chemistry model system MECO(n) – Part 1: Description of the limited-area atmospheric chemistry model COSMO/MESSy, Geoscientific Model Development, 5, 87–110, https://doi.org/10.5194/gmd-5-87-2012, 2012.

Khairoutdinov, M., Randall, D., and DeMott, C.: Simulations of the atmospheric general circulation using a cloud-resolving model as a superparameterization of physical processes, Journal of the Atmospheric Sciences, 62, 2136–2154, https://doi.org/10.1175/JAS3453.1, 2005.

Khairoutdinov, M., DeMott, C., and Randall, D.: Evaluation of the simulated interannual and subseasonal variability in an AMIP-Style simulation using the CSU multiscale modeling framework, Journal of Climate, 21, 413–431, https://doi.org/10.1175/2007JCLI1630.1, 2008.

Khairoutdinov, M. F. and Randall, D. A.: A cloud resolving model as a cloud parameterization in the NCAR Community Climate System Model: Preliminary results, Geophysical Research Letters, 28, 3617–3620, https://doi.org/10.1029/2001GL013552, 2001.

Khairoutdinov, M. F. and Randall, D. A.: Cloud resolving modeling of the ARM summer 1997 IOP: Model formulation, results, uncertainties, and sensitivities, Journal of the Atmospheric Sciences, 60, 607–625, https://doi.org/10.1175/1520-0469(2003)060<0607:CRMOTA>2.0.CO;2, 2003.

Knutti, R., Stocker, T. F., Joos, F., and Plattner, G. K.: Constraints on radiative forcing and future climate change from observations and climate model ensembles, Nature, 416, 719–723, https://doi.org/10.1038/416719a, 2002.

Kodama, C., Yamada, Y., Noda, A. T., Kikuchi, K., Kajikawa, Y., Nasuno, T., Tomita, T., Yamaura, T., Takahashi, H. G., Hara, M., Kawatani, Y., Satoh, M., and Sugi, M.: A 20-Year Climatology of a NICAM AMIP-Type Simulation, Journal of the Meteorological Society of Japan. Ser. II, 93, 393–424, https://doi.org/10.2151/jmsj.2015-024, 2015.

Kooperman, G. J., Pritchard, M. S., Burt, M. A., Branson, M. D., and Randall, D. A.: Robust effects of cloud superparameterization on simulated daily rainfall intensity statistics across multiple versions of the Community Earth System Model, Journal of Advances in Modeling Earth Systems, 8, 140–165, https://doi.org/10.1002/2015MS000574, 2016.

Lauer, A. and Hamilton, K.: Simulating Clouds with Global Climate Models: A Comparison of CMIP5 Results with CMIP3 and Satellite Data, Journal of Climate, 26, 3823–3845, https://doi.org/10.1175/JCLI-D-12-00451.1, 2013.

Loeb, N. G., Wielicki, B. A., Doelling, D. R., Smith, G. L., Keyes, D. F., Kato, S., Manalo-Smith, N., and Wong, T.: Toward optimal closure of the Earth's top-of-atmosphere radiation budget, Journal of Climate, 22, 748–766, 2009.

Lohmann, U. and Roeckner, E.: Design and performance of a new cloud microphysics scheme developed for the ECHAM general circulation model, Climate Dynamics, 12, 557–572, https://doi.org/10.1007/s003820050128, 1996.

Mace, G. G.: Cloud properties and radiative forcing over the maritime storm tracks of the Southern Ocean and North Atlantic derived from A-Train, Journal of Geophysical Research: Atmospheres, 115, https://doi.org/10.1029/2009JD012517, 2010.

Maher, P., Vallis, G. K., Sherwood, S. C., Webb, M. J., and Sansom, P. G.: The Impact of Parameterized Convection on Climatological Precipitation in Atmospheric Global Climate Models, Geophysical Research Letters, 45, 3728–3736, https://doi.org/10.1002/2017GL076826, 2018.

Marchand, R. and Ackerman, T.: An analysis of cloud cover in multiscale modeling framework global climate model simulations using 4 and 1 km horizontal grids, Journal of Geophysical Research-atmospheres, 115, https://doi.org/10.1029/2009JD013423, 2010.

Marchand, R., Haynes, J., Mace, G. G., Ackerman, T., and Stephens, G.: A comparison of simulated cloud radar output from the multiscale modeling framework global climate model with CloudSat cloud radar observations, Journal of Geophysical Research: Atmospheres, 114, https://doi.org/10.1029/2008JD009790, 2009.

Matsui, T., Chern, J.-D., Tao, W.-K., Lang, S., Satoh, M., Hashino, T., and Kubota, T.: On the Land–Ocean Contrast of Tropical Convection and Microphysics Statistics Derived from TRMM Satellite Signals and Global Storm-Resolving Models, Journal of Hydrometeorology, 17, 1425–1445, https://doi.org/10.1175/JHM-D-15-0111.1, 2016.

Mauritsen, T., Stevens, B., Roeckner, E., Crueger, T., Esch, M., Giorgetta, M., Haak, H., Jungclaus, J., Klocke, D., Matei, D., Mikolajewicz, U., Notz, D., Pincus, R., Schmidt, H., and Tomassini, L.: Tuning the climate of a global model, Journal of Advances In Modeling Earth Systems, 4, https://doi.org/10.1029/2012MS000154, 2012.

Minghuai, W., E., L. V., Steven, G., Mikhail, O., P., S. D., Heng, X., Xiaohong, L., Philip, R., and Zhun, G.: A multiscale modeling framework model (superparameterized CAM5) with a higher-order turbulence closure: Model description and low-cloud simulations, Journal of Advances in Modeling Earth Systems, 7, 484–509, https://doi.org/10.1002/2014MS000375, 2015.

Miura, H., Satoh, M., Nasuno, T., Noda, A. T., and Oouchi, K.: A Madden-Julian Oscillation Event Realistically Simulated by a Global Cloud-Resolving Model, Science, 318, 1763–1765, https://doi.org/10.1126/science.1148443, 2007.

Miyakawa, T., Satoh, M., Miura, H., Tomita, H., Yashiro, H., Noda, A. T., Yamada, Y., Kodama, C., Kimoto, M., and Yoneyama, K.: Madden-Julian Oscillation prediction skill of a new-generation global model demonstrated using a supercomputer, Nature Communications, 5, 3769, https://doi.org/10.1038/ncomms4769, 2014.

Miyamoto, Y., Kajikawa, Y., Yoshida, R., Yamaura, T., Yashiro, H., and Tomita, H.: Deep moist atmospheric convection in a subkilometer global simulation, Geophysical Research Letters, 40, 4922–4926, https://doi.org/10.1002/grl.50944, 2013.

Nordeng, T. E.: Extended versions of the convective parametrization scheme at ECMWF and their impact on the mean and transient activity of the model in the tropics., Technical Momorandum 206, ECMWF Research Department, European Centre for Medium Range Weather Forecasts, Reading, UK, 1994.

O'Dell, C. W., Wentz, F. J., and Bennartz, R.: Cloud Liquid Water Path from Satellite-Based Passive Microwave Observations: A New Climatology over the Global Oceans, Journal of Climate, 21, 1721–1739, https://doi.org/10.1175/2007JCLI1958.1, 2008.

Pritchard, M. S. and Somerville, R. C. J.: Assessing the Diurnal Cycle of Precipitation in a Multi-Scale Climate Model, Journal of Advances In Modeling Earth Systems, 1, 12, 2009a.

Pritchard, M. S. and Somerville, R. C. J.: Empirical orthogonal function analysis of the diurnal cycle of precipitation in a multi-scale climate model, Geophysical Research Letters, 36, https://doi.org/10.1029/2008GL036964, l05812, 2009b.

Probst, P., Rizzi, R., Tosi, E., Lucarini, V., and Maestri, T.: Total cloud cover from satellite observations and climate models, ATMOSPHERIC RESEARCH, 107, 161–170, https://doi.org/10.1016/j.atmosres.2012.01.005, 2012.

Roeckner, E., Brokopf, R., Esch, M., Giorgetta, M., Hagemann, S., Kornblueh, L., Manzini, E., Schlese, U., and Schulzweida, U.: Sensitivity of simulated climate to horizontal and vertical resolution in the ECHAM5 atmosphere model, Journal of Climate, 19, 3771–3791, https://doi.org/10.1175/JCLI3824.1, 2006.

Sato, T., Miura, H., Satoh, M., Takayabu, Y. N., and Wang, Y.: Diurnal Cycle of Precipitation in the Tropics Simulated in a Global Cloud-Resolving Model, Journal of Climate, 22, 4809–4826, https://doi.org/10.1175/2009JCLI2890.1, 2009.

Stephens, G. L., L'Ecuyer, T., Forbes, R., Gettelmen, A., Golaz, J.-C., Bodas-Salcedo, A., Suzuki, K., Gabriel, P., and Haynes, J.: Dreary state of precipitation in global models, Journal of Geophysical Research: Atmospheres, 115, https://doi.org/10.1029/2010JD014532, 2010.

Stubenrauch, C. J., Rossow, W. B., Kinne, S., Ackerman, S., Cesana, G., Chepfer, H., Di Girolamo, L., Getzewich, B., Guignard, A., Heidinger, A., Maddux, B. C., Menzel, W. P., Minnis, P., Pearl, C., Platnick, S., Poulsen, C., Riedi, J., Sun-Mack, S., Walther, A., Winker, D., Zeng, S., and Zhao, G.: Assessment of Global Cloud Datasets from Satellites: Project and Database Initiated by the GEWEX Radiation Panel, Bulletin of the American Meteorological Society, 94, 1031–1049, https://doi.org/10.1175/BAMS-D-12-00117.1, 2013.

Subramanian, A., Weisheimer, A., Palmer, T., Vitart, F., and Bechtold, P.: Impact of stochastic physics on tropical precipitation in the coupled ECMWF model, Quarterly Journal of the Royal Meteorological Society, 143, 852–865, https://doi.org/10.1002/qj.2970, 2017.

Sui, C.-H., Lau, K.-M., Takayabu, Y. N., and Short, D. A.: Diurnal Variations in Tropical Oceanic Cumulus Convection during TOGA COARE, Journal of the Atmospheric Sciences, 54, 639–655, https://doi.org/10.1175/1520-0469(1997)054<0639:DVITOC>2.0.CO;2, 1997.

Sui, C.-H., Li, X., and Lau, K.-M.: Radiative–Convective Processes in Simulated Diurnal Variations of Tropical Oceanic Convection, Journal of the Atmospheric Sciences, 55, 2345–2357, https://doi.org/10.1175/1520-0469(1998)055<2345:RCPISD>2.0.CO;2, 1998.

Suzuki, K., Stephens, G., Bodas-Salcedo, A., Wang, M., Golaz, J.-C., Yokohata, T., and Koshiro, T.: Evaluation of the Warm Rain Formation Process in Global Models with Satellite Observations, Journal of the Atmospheric Sciences, 72, 3996–4014, https://doi.org/10.1175/JAS-D-14-0265.1, 2015.

Tao, W. K., Chern, J. D., Atlas, R., Randall, D., Khairoutdinov, M., Li, J. L., Waliser, D. E., Hou, A., Lin, X., Peters-Lidard, C., Lau, W., Jiang, J., and Simpson, J.: A Multiscale Modeling System: Developments, Applications, and Critical Issues, Bulletin of the American Meteorological Society, 90, 515–534, https://doi.org/10.1175/2008BAMS2542.1, 2009.

Taylor, K. E.: Summarizing multiple aspects of model performance in a single diagram., Journal of Geophysical Research-atmospheres, 106, 7183–7192, https://doi.org/10.1029/2000JD900719, 2001.

Tiedtke, M.: A Comprehensive Mass Flux Scheme For Cumulus Parameterization In Large-scale Models, Monthly Weather Review, 117, 1779–1800, https://doi.org/10.1175/1520-0493(1989)117<1779:ACMFSF>2.0.CO;2, 1989.

Tost, H., Joeckel, P., and Lelieveld, J.: Influence of different convection parameterisations in a GCM, Atmospheric Chemistry and Physics, 6, 5475–5493, 2006.

5   Tulich, S. N.: A strategy for representing the effects of convective momentum transport in multiscale models: Evaluation using a new superparameterized version of the Weather Research and Forecast model (SP-WRF), Journal of Advances in Modeling Earth Systems, 7, 938–962, https://doi.org/10.1002/2014MS000417, 2015.

Wang, M., Ghan, S., Easter, R., Ovchinnikov, M., Liu, X., Kassianov, E., Qian, Y., Gustafson, W. I., Larson, V. E., Schanen, D. P., Khairoutdinov, M., and Morrison, H.: The multi-scale aerosol-climate model PNNL-MMF: model description and evaluation, Geoscientific Model

10   Development, 4, 137–168, https://doi.org/10.5194/gmd-4-137-2011, 2011a.

Wang, M., Ghan, S., Ovchinnikov, M., Liu, X., Easter, R., Kassianov, E., Qian, Y., and Morrison, H.: Aerosol indirect effects in a multi-scale aerosol-climate model PNNL-MMF, Atmos. Chem. Phys., 11, 5431–5455, https://www.atmos-chem-phys.net/11/5431/2011/, 2011b.

Wielicki, B. A., Barkstrom, B. R., Harrison, E. F., III, R. B. L., Smith, G. L., and Cooper, J. E.: Clouds and the Earth's Radiant Energy System (CERES): An Earth Observing System Experiment, Bulletin of the American Meteorological Society, 77, 853–868,

15   https://doi.org/10.1175/1520-0477(1996)077<0853:CATERE>2.0.CO;2, 1996.

Yang, S. and Smith, E. A.: Mechanisms for Diurnal Variability of Global Tropical Rainfall Observed from TRMM, Journal of Climate, 19, 5190–5226, https://doi.org/10.1175/JCLI3883.1, 2006.

Yashiro, H., Kajikawa, Y., Miyamoto, Y., Yamaura, T., Yoshida, R., and Tomita, H.: Resolution Dependence of the Diurnal Cycle of Precipitation Simulated by a Global Cloud-System Resolving Model, SOLA, 12, 272–276, https://doi.org/10.2151/sola.2016-053, 2016.

20   Zhang, G. J. and McFarlane, N. A.: Sensitivity of Climate Simulations To the Parameterization of Cumulus Convection In the Canadian Climate Center General-circulation Model, Atmosphere-ocean, 33, 407–446, 1995.

Zhang, T., Zhang, M., Lin, W., Lin, Y., Xue, W., Yu, H., He, J., Xin, X., Ma, H.-Y., Xie, S., and Zheng, W.: Automatic tuning of the Community Atmospheric Model (CAM5) by using short-term hindcasts with an improved downhill simplex optimization method, Geoscientific Model Development, 11, 5189–5201, https://doi.org/10.5194/gmd-11-5189-2018, https://www.geosci-model-dev.net/11/5189/2018/,

25   2018.

Zhang, Y., Klein, S. A., Liu, C., Tian, B., Marchand, R. T., Haynes, J. M., McCoy, R. B., Zhang, Y., and Ackerman, T. P.: On the diurnal cycle of deep convection, high-level cloud, and upper troposphere water vapor in the Multiscale Modeling Framework, Journal of Geophysical Research: Atmospheres, 113, https://doi.org/10.1029/2008JD009905, 2008.
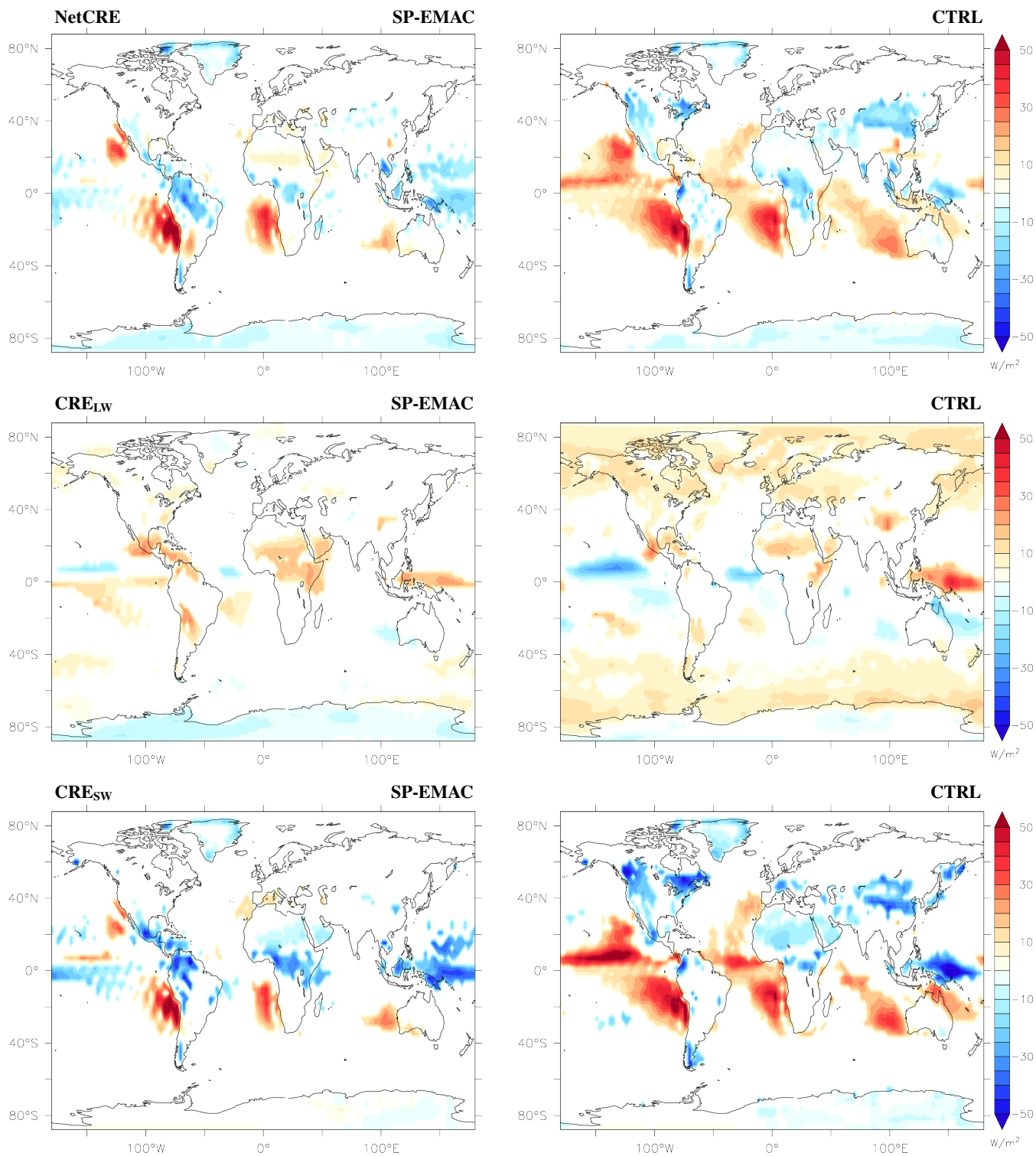
Figure 8. Differences in simulated minus observed cloud radiative effects at TOA (net - upper row, longwave - middle row, shortwave - lower row). Results for SP-EMAC ensemble (left column) and CTRL (right column) are shown comparing to global observations (CERES). Colored areas show only regions with significant differences in precipitation (analysed with t-Tests on a significance level of 90%).
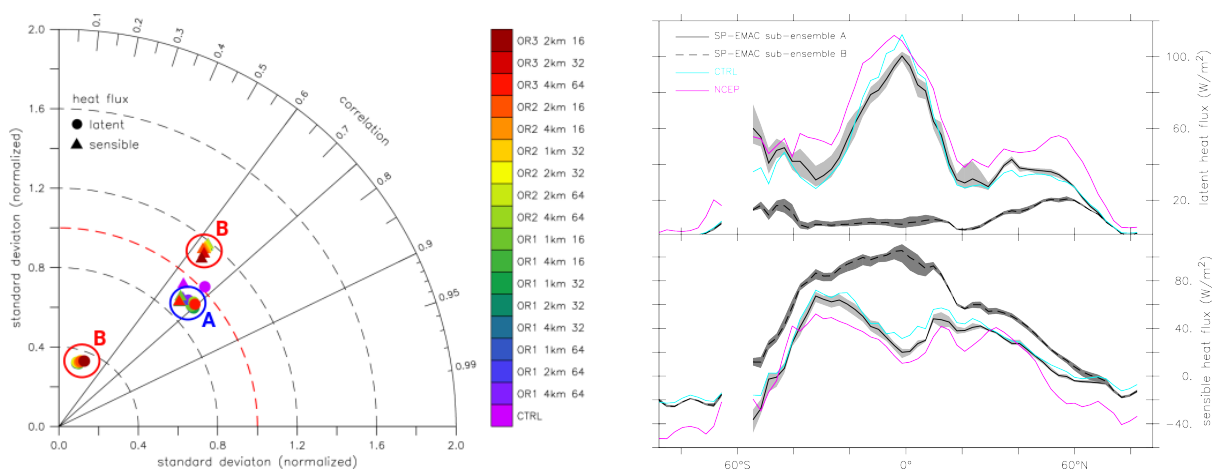
Figure 9. Global Taylor diagram (left) and zonal plots of sensible and latent heat fluxes over land (right). Sub-ensembles are highlighted in the Taylor diagram with blue and red circles. For comparison purposes reanalysis data of NCEP is taken to compare all simulations.
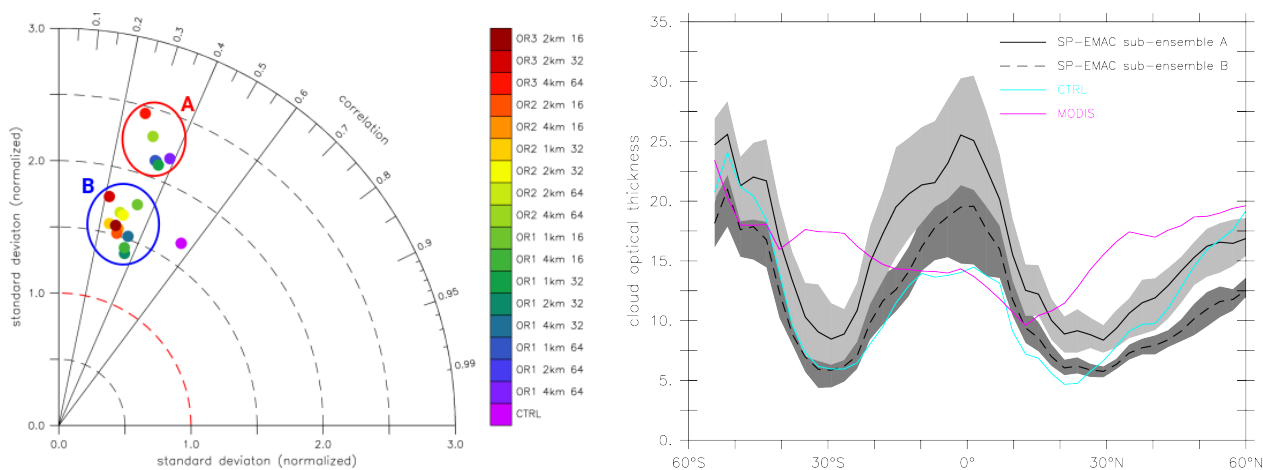
Figure 10. Global Taylor diagram (left) and zonal plots of cloud optical thickness over land (right). The performance of the sub-ensembles are highlighted in the Taylor diagram with blue and red ellipses. Observational data is taken from MODIS retrievals.